Search for vector-like leptons at the Large Hadron Collider

A thesis submitted towards partial fulfilment of

BS-MS Dual Degree Programme

by

Santpur Sai Neha

under the guidance of

Prof. Sourabh Dube

Indian Institute of Science Education and Research Pune

Certificate

This is to certify that this thesis entitled "Search for vector-like leptons at the Large Hadron Collider" submitted towards the partial fulfilment of the BS-MS dual degree programme at the Indian Institute of Science Education and Research Pune represents original research carried out by Santpur Sai Neha at Indian Institute of Science Education and Research Pune, under the supervision of Prof. Sourabh Dube during the academic year 2015-2016.

Student

SANTPUR SAI NEHA

Supervisor

PROF. SOURABH DUBE

Declaration

I hereby declare that the matter embodied in the report entitled Search for vector-like leptons at the Large Hadron Collider are the results of the investigations carried out by me at the Department of Physics, Indian Institute of Science Education and Research Pune, under the supervision of Prof. Sourabh Dube and the same has not been submitted elsewhere for any other degree.

Student

Santpur Sai Neha

Supervisor

Prof. Sourabh Dube

Acknowledgements

Firstly, I would like to express my extreme gratitude to Prof. Sourabh Dube for guiding me for over 2.5 years. Thanks to him for being very patient and super supportive during this entire time, specifically during my thesis. I am also grateful to Prof. Seema Sharma for valuable inputs through out the project. Special thanks to the Rutgers Multilepton group, specially Prof. Sunil Somalwar, for all the encouragement and suggestions.

Thanks to all my EHEP group members especially Anshul, Kunal and Shubhanshu with whom I grew in this field! Thanks to them for being so supportive and helping. I would particularly like to thank Shubhanshu for sharing his office space, helping me with the background samples and also for being the 3 A.M. friend!

Last but not the least, I owe a great deal to my family. Thanks to mom, dad, Manu, Hrishi and Shankar for supporting me not only emotionally but also very actively in my research. Thanks for always being interested in what I and physics are up to! Also, thanks to them for proof-reading my thesis.

Abstract

I study the scope of discovering vector-like leptons at the Large Hadron Collider. Unlike the Standard Model, vector-like leptons are non-chiral. Many beyond the Standard Model theories like composite Higgs model, warped extra-dimensions, supersymmetry predict the existence of such leptons. I studied vector-like lepton model in a multilepton final state using an ATLAS 8 TeV search result. I exclude vector-like leptons with masses below 150-280 GeV depending on specific model parameters. I study the doublet model at center of mass energy of 13 TeV using a multilepton final state. I design signal regions to maximize signal to background ratio and I make predictions about the sensitivity of multilepton final state to the vector-like lepton model. The optimized signal region corresponds to 2l-tau, onZ channel with m_{eff} $\geq$600 GeV. Using this signal region, I predict 95% CL exclusion limit for a luminosity of 20 fb^{-1}. I excluded vector-like leptons in the doublet model having masses below 365 GeV.

Contents

1 Introduction **4**

1.1 Inadequacies of the Standard Model 5

1.2 Beyond Standard Model physics 6

2 Vector-like lepton model **8**

2.1 Fourth generation of matter 9

2.2 What are vector-like fermions? 10

2.3 Models 11

2.3.1 Doublet model 11

2.3.2 Singlet B model 14

2.3.3 Singlet A model 15

2.4 Previous searches 17

3 Analysis strategy **18**

4 Simulation of signal and background samples **21**

4.1 Signal samples 22

4.1.1 Model implementation 23

4.2 SM Background samples 25

5 Analysis for LHC Run I data **27**

5.1 Model testing using an ATLAS 8 TeV search 27

5.2 Event selection 29

5.2.1 Event efficiency 30

5.2.2 Signal regions . . . 31
5.3 Kinematic distributions . . . 33
5.4 Interpretation of the results . . . 34
5.4.1 Doublet model . . . 34
5.4.2 Singlet B model . . . 35
5.4.3 Singlet A model . . . 36
5.4.4 Summary . . . 36

6 LHC Run II prospects **38**
6.1 Event pre-selection . . . 38
6.2 Background estimation . . . 39
6.3 Signal regions . . . 40
6.4 Optimization of the search . . . 42
6.5 Prediction of exclusion limits . . . 46

7 Summary **49**

References **50**

Chapter 1

Introduction

The Standard Model of particle physics has not only successfully accounted for most of the experimental results but has also rightly predicted many new phenomena including the existence of top quark, tau neutrino, W, Z and the Higgs bosons. This theory incorporates the strong, weak and electromagnetic forces in a single framework. In late 1960s, Abdus Salam, Steven Weinberg and Sheldon Glashow merged the electromagnetic and weak forces into a single electroweak force with the inclusion of the Higgs mechanism. The strong force was added to this description in early 1970s, thus completing the Standard Model as we know it today [1–5].

This theory includes fundamental particles and gives a description of the interactions between them. The particle content of the Standard Model is given in Figure 1.1. There are 61 fundamental particles comprising of 12 leptons, 36 quarks, 12 gauge bosons and 1 Higgs boson. The quarks and leptons make up the matter content of the universe and the gauge bosons mediate the interactions between them. The stable matter in the universe is dominated by the up, down quarks and the electron. The photon, γ, mediates the electromagnetic force and W^+, W^-, Z bosons mediate the weak force. The gluon, g, is the carrier of the strong force. The Higgs boson, a scalar boson, arises due to the spontaneous symmetry breaking of the electroweak theory. All the massive particles [1] in the Standard Model acquire their mass upon interaction with the Higgs field [7, 8].

[1] Neutrinos are massless in the Standard Model of course.

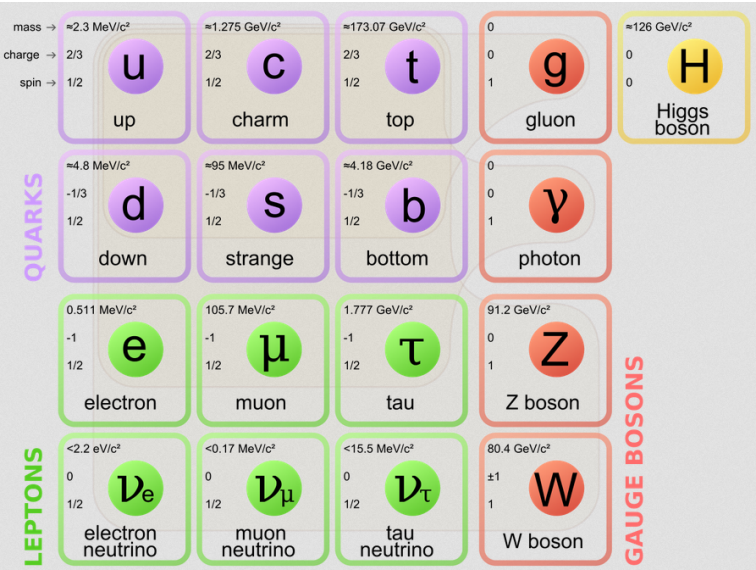

Figure 1.1: Standard Model particles [6]

1.1 Inadequacies of the Standard Model

The Standard Model is the most consistent theory of fundamental particles we have today [9]. Though successful, it is not a complete description of elementary particles and their interactions [10]. There are outstanding problems with this model and I will mention a few here [11].

1. *Gravitational interaction*: The Standard Model incorporates weak, electromagnetic and strong forces but does not include the gravitational interaction in its framework.

2. *Neutrino masses*: The neutrinos in the Standard Model are massless. But experimentally, neutrino oscillations were observed at Super-Kamiokande experiment [12] and the Sudbury Neutrino Observatory (SNO) [13]. Neutrino oscillations imply that a neutrino of one flavor can convert into a neutrino of other flavor. For example, SNO experiment observed the conversion of ν_e from Sun into ν_μ and ν_τ. The observation of neutrino oscillations requires at least two neutrinos to have a non-zero mass [14]. This is in conflict with the Standard Model's prediction of massless neutrinos.

3. *Dark matter*: The galaxy rotation curves provide the evidence for the existence of dark matter [15]. The word *dark* in its name indicates that it is electromagnetically

neutral and hence cannot be detected using the standard electromagnetic imaging techniques [16]. While the exact nature of dark matter is unknown, what is known about the dark matter is that it interacts only through gravity and probably the weak force. The Standard Model doesn't provide any viable dark matter candidate.

4. *Matter-Antimatter asymmetry*: The observable universe is predominantly composed of matter and not anti-matter. The Standard Model cannot account for this imbalance.

5. *Hierarchy problem*: In the Standard Model, mass of the Higgs boson acquires quadratically divergent contributions from quantum corrections. The ATLAS and the CMS experiments discovered the Higgs boson with mass of around 125 GeV [17, 18]. The parameters of the Standard Model need to be fine-tuned in order to obtain a finite mass for the Higgs boson. There is no theoretical motivation in the Standard Model for this fine-tuning.

6. *Why three generations of matter*: The three generations of quarks and leptons are experimentally established and they neatly fit into the $\mathrm{SU}(3)_C \times \mathrm{SU}(2)_Y \times \mathrm{U}(1)_Y$ description of the Standard Model. But there is no a priori reason why we do not expect four or more generations.

7. *Mass hierarchy between three generations of matter*: The masses of the three generations of quarks and leptons are different by orders of magnitude. For example, electron's mass is 0.5 MeV while the tau's mass is 1.7 GeV. The Standard Model doesn't account for this disparity.

1.2 Beyond Standard Model physics

Many theories beyond the Standard Model (BSM) are proposed to resolve one or many of the above mentioned issues. Some of the well-studied ones are supersymmetry, seesaw mechanism, extra-dimensions, vector-like fermion models, compositeness and Higgs doublet model. Supersymmetry proposes a symmetry between fermions and bosons [19]. The supersymmetric transformation acting on a fermionic state results in a bosonic one and

viceversa. Thus for every Standard Model particle, there exists a supersymmetric partner with spin-$\frac{1}{2}$ difference. This theory naturally solves the hierarchy problem, and also provides a viable dark-matter candidate. The seesaw mechanism addresses the issue of massive neutrinos [20]. The extra-dimension models propose extra spatial dimensions in addition to the regular four-dimensional spacetime [21]. These models explain why gravity is so weak compared to the other three forces in nature and also predict the existence of massive gravitons.

The Vector-like fermion models predict additional fermions, and are described in detail in Chapter 2.

Chapter 2

Vector-like lepton model

One simple extension of Standard Model (SM) is the inclusion of new vector-like leptons. Models with these new particles can explain the mass hierarchy between the three generations of matter [22]. This hierarchy refers to the electron mass being 0.5 MeV while the mass of tau lepton is 1.7 GeV. In vector-like lepton models, the Standard Model leptons acquire mass upon mixing with these new leptons and this mixing explains the mass hierarchy between different generations. They feature in many BSM theories including composite Higgs model [23,24], warped extra-dimensions [25,26] and supersymmetry [27].

In December 2015, the ATLAS and the CMS collaborations observed a slight deviation from the Standard Model prediction [28,29]. They reported a slight excess in the diphoton invariant mass spectrum at around 750 GeV. If this excess is confirmed as the presence of a new particle, then this might be the first hint of beyond the Standard Model physics. One of the BSM models that can explain this resonance is the vector-like lepton model [30].

The vector-like leptons are different from the Standard Model leptons. Before I discuss what they are, I will examine the case for the existence of additional SM like leptons in nature.

2.1 Fourth generation of matter

Experimentally, we discovered three generations of matter and they fit neatly into the Standard Model framework. But a natural question to ask is, are there additional fermions? While nothing prevents having more fermions in nature, there are severe experimental constraints on a SM like fourth generation. The CMS and ATLAS experiments have placed a lower bound on the mass of fourth generation quarks to be around 480-685 GeV [31–34] depending on the specifics of the model being probed. Existence of such a massive particle would have noticable implications on electroweak precision observables [35]. This new particle would couple to W, Z and Higgs resulting in measurable deviations from SM predictions of the their mass, production cross section, branching ratio, etc.

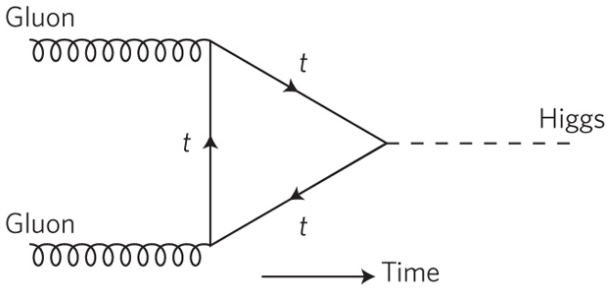

Figure 2.1: Higgs production through gluon-gluon fusion. Here, the Higgs boson is produced from gluons through a top quark loop. If a SM-like fourth generation of matter exists, then it would also contribute to the Higgs production through a fermion loop, similar to the top quark.

For illustration purposes, let us consider the Higgs boson production through gluon fusion. In Standard Model, one of the ways this fusion takes place is through a fermion loop as shown in Figure 2.1. If a new up-type quark with mass > 650 GeV existed, then it would contribute to this process similar to the top quark. As the coupling to higgs boson is proportional to the mass of the particle, these new particles will enhance the Higgs production cross section. This would imply that the measured Higgs production cross section would be higher than the SM prediction. Using LHC Run I data, the CMS experiment obtained the ratio of measured Higgs cross section to that of the SM to be 1.00 ± 0.13 [36]. Thus we see that the measurement shows consistency with the Standard

Model.

Similarly, the L3 collaboration puts a lower bound on the masses of heavy leptons to be 100.2 GeV [37]. Therefore, if a fourth generation lepton with mass more than a 100 GeV existed, it would also contribute to the enhancement of Higgs cross section like above and the same argument holds true. In general, SM predictions of various electroweak precision observables is in sync with the data. Though the existence of SM like generation of quarks and leptons is not completely ruled out, it is severely constrained.

2.2 What are vector-like fermions?

The fermions in the Standard Model are chiral. This implies that the left-handed fermions and the right-handed fermions transform differently under the symmetries of the theory. For example, the weak charged current interacts with the left-handed fermions but not the right-handed fermions. This asymmetric interaction of left and right handed fermions in the Standard Model makes it a chiral theory.

The particles whose left and right handed components transform similarly under the symmetries of the theory are non-chiral and are referred to as vector-like particles [22, 38–41]. For example, the interaction of weak charged current with left and right handed vector-like fermions is similar. As a result, the vector-like fermion's interaction with the W, Z and the Higgs boson is different from Standard Model fermion. One important consequence is that their contribution to the electroweak precision observables decouples or decreases as their mass increases [41]. This implies that a heavy vector-like fermion might exist in nature that does not result in measurable deviations in these observables from SM predictions. Therefore, these particles are less constrained than extra SM like fermions. Only direct searches for vector-like fermions can be used to constrain these models.

Vector-like lepton model is not a single model but a class of models (like supersymmetry refers to a broad range of models with large parameter space). In the next section, I introduce the different vector-like lepton models that I have probed.

2.3 Models

Vector-like leptons (VLL) are spin $\frac{1}{2}$ particles whose masses are expected to be higher than the SM leptons. As they are leptons, they do not have any color charge [22, 38–41]. Just like the SM leptons, these vector-like leptons can be electromagnetically charged or neutral. The vector-like lepton models are a simple extension to the Standard Model where we add vector-like leptons to the SM generations. This results in vector-like leptons having lepton numbers similar to the SM generation that they are added to. For example, if we add a vector-like electron (e') to the first generation of SM leptons, then this e' would have a corresponding electron number (L_e) and this would be conserved in all its interactions.

The Vector-like lepton models can be broadly classified into two categories: *singlet* and the *doublet VLL models*. From an experimental perspective, the difference between these models is that the singlet VLL model allows only charged vector-like leptons while the doublet VLL model allows charged and neutral vector-like leptons. For example, singlet model adds only one charged vector-like electron (or muon or tau) and its antiparticle to the first generation. On the other hand, the doublet model adds one charged vector-like electron (or muon or tau), its antiparticle and one neutral vector-like neutrino along with its antiparticle. Therefore, the singlet model has two new particles where as the doublet model has four.

All the models for my study are minimal extensions of the Standard Model where only one generation of vector-like leptons are added. In principle, we can have more generations of vector-like leptons too. I explored two types of singlet VLL models (labelled as A and B in subsequent discussion) and one doublet VLL model. I will briefly discuss each of these models including the new particles and their decays in the following subsections.

2.3.1 Doublet model

The doublet VLL model adds a vector-like tau τ'^{-}, its antiparticle τ'^{+} and a neutrino ν'_{τ} along with its antiparticle $\bar{\nu}'_{\tau}$ to the Standard Model. This model and the singlet B model

discussed below are described in Ref. [41]. In this model, it is assumed that $m(\tau')$=$m(\nu'_\tau)$ i.e. the vector-like tau and the corresponding neutrino are degenerate. The production channel for the vector-like leptons in this model refers to pair-production ($\tau'^{+}\tau'^{-}$,$\nu'_\tau\bar{\nu}'_\tau$) or associated production ($\tau'^{+}\nu'_\tau$, $\tau'^{-}\bar{\nu}'_\tau$). The production cross sections of these channels for the Large Hadron Collider at center of mass energies of 8 and 13 TeV is displayed in Figure 2.2.

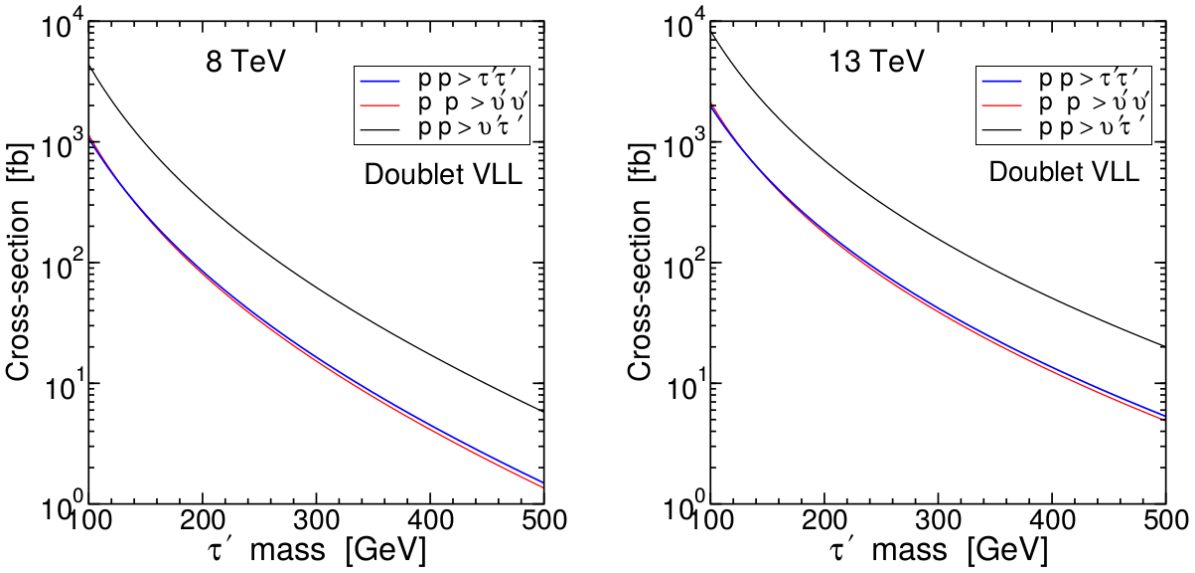

Figure 2.2: Production cross section for different channels as a function of mass of vector-like leptons (doublet VLL model) [41]

These new particles would be unstable and short-lived, and decay into Standard Model particles. In the doublet VLL model, the vector-like tau couples to Z and Higgs bosons but not the W boson. This implies the τ'^{-} can decay into $Z\tau^{-}$ and $H\tau^{-}$ and the Feynman diagrams for this decay are shown in Figure 2.3.The branching fraction for these decays is shown in Figure 2.4. We observe that B($\tau'^{-} \rightarrow H\tau^{-}$) increases as $m(\tau')$ increases and asymptotically reaches 0.5.

On the other hand, ν'_τ only decays into a W boson and a tau lepton. The Feynman diagram for this decay is given in Figure 2.5. The Branching ratio for this decay is 100% irrespective of the mass of ν'_τ.

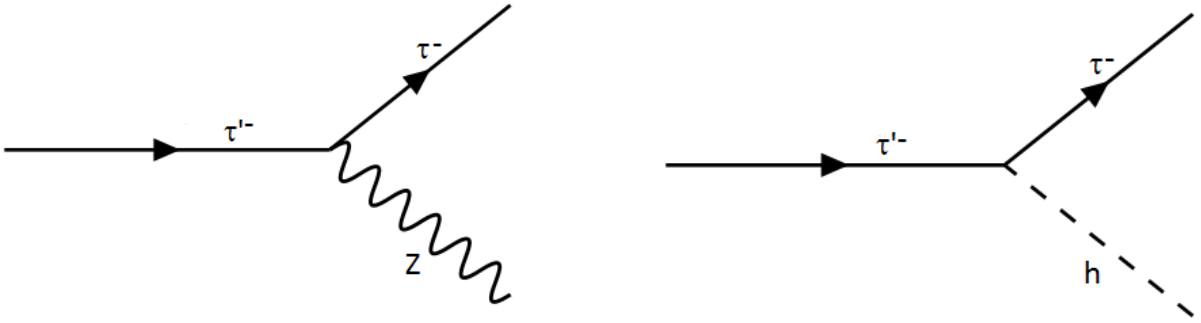

Figure 2.3: Feynman diagrams for the decays of τ'^{-} in the doublet VLL model

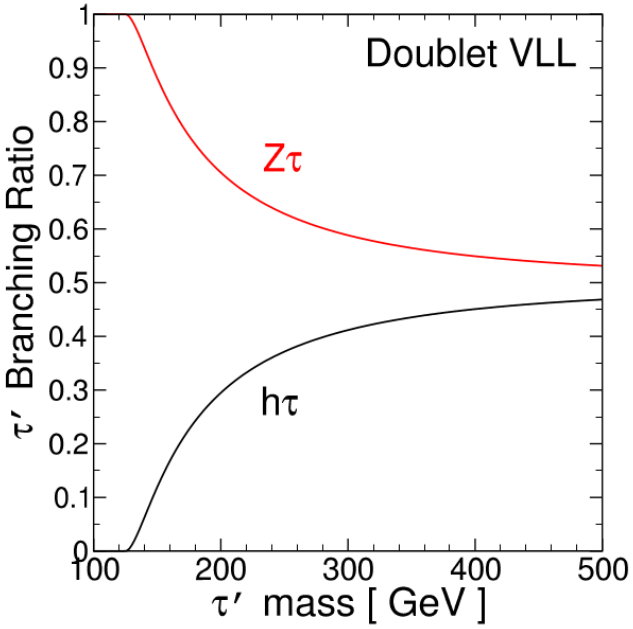

Figure 2.4: Branching ratio of different decay modes of τ' as a function of its mass (doublet VLL model) [41]

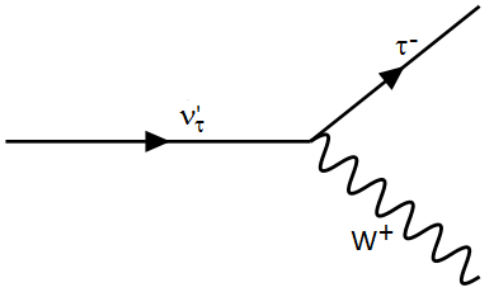

Figure 2.5: Feynman diagrams for the decay of ν'_τ in the doublet VLL model

2.3.2 Singlet B model

In this singlet VLL model, we have a vector-like tau (τ'^-) and its antiparticle (τ'^+) added to the third SM generation [41]. Unlike the doublet VLL model, this model does not predict the existence of a new neutrino i.e. no ν'_τ in this model. The production of vector-like leptons in this model is only through pair production of $\tau'^+\tau'^-$. The production cross section as a function of mass is depicted in Figure 2.6.

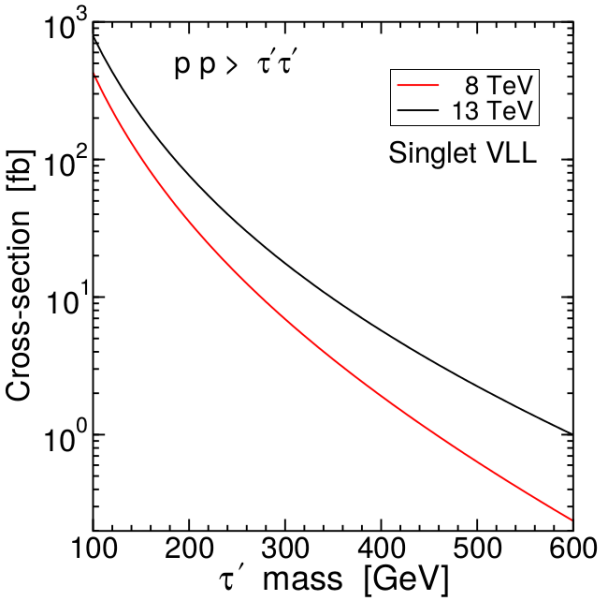

Figure 2.6: Production cross section as a function of mass of vector-like leptons (singlet B VLL model) [41]

Apart from the above mentioned difference , another important distinguishing factor between the singlet and the doublet VLL model is as follows. The τ'^- in the singlet model couples with the W boson in addition to Z and the Higgs bosons in SM. Therefore, in this model the τ'^- decays into $W^-\nu_\tau$, $Z\tau^-$ and $H\tau^-$, as depicted in Figure 2.7. The branching ratio corresponding to each of these decay modes is presented in Figure 2.8. As expected, the branching fraction, B($\tau'^- \to H\tau^-$), increases with $m(\tau')$. As $m(\tau')$ increases further, B($\tau'^- \to W^-\nu_\tau$) asymptotically tends to 0.5 while both B($\tau'^- \to Z\tau^-$) and B($\tau'^- \to H\tau^-$) asymptotically reach 0.25.

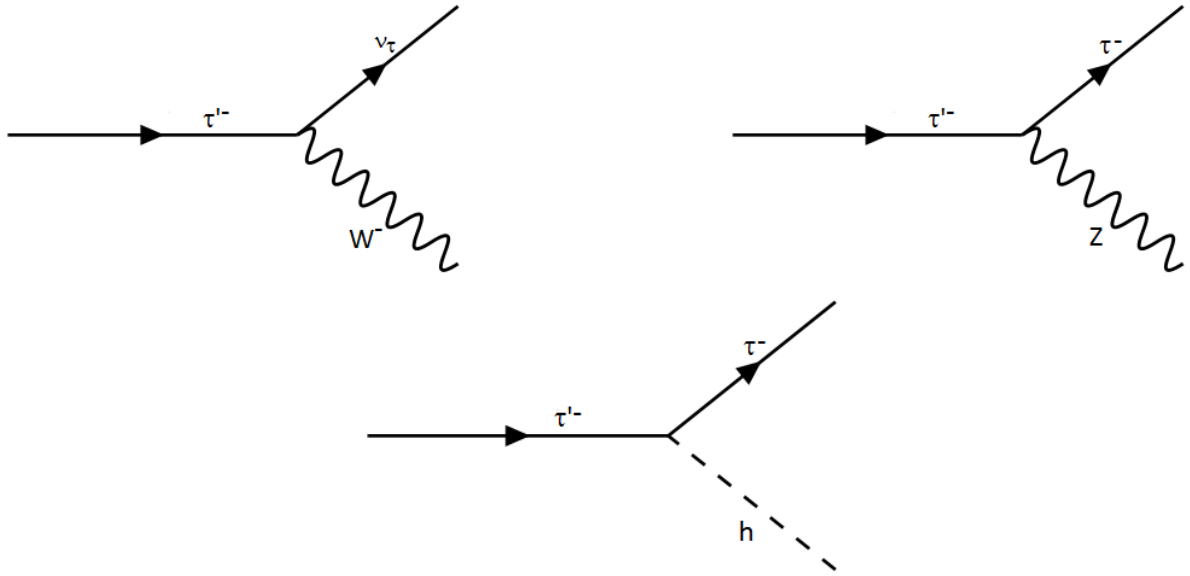

Figure 2.7: Feynman diagrams for the decays of τ'^{-} in Singlet B model

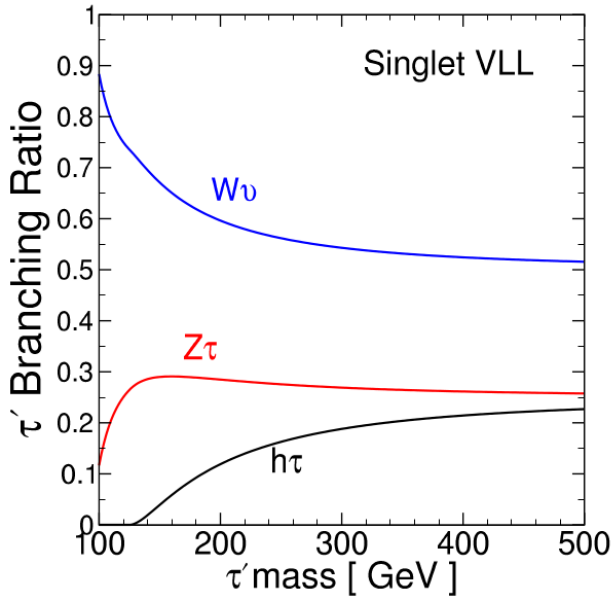

Figure 2.8: Branching ratio of different decay modes of τ' as a function of its mass (Singlet B model) [41]

2.3.3 Singlet A model

This particular model is described in Ref. [42]. Here, vector-like electron, e'^{-}, and its anti-particle, e'^{+}, are added to the Standard Model. In this model, I consider vector-like electrons as they couple to SM bosons and the first generation leptons (e,ν_e). This gives us a different event topology from the doublet and singlet B model to search for vector-

like particles. The new particles in the other two models decay and result in taus and these taus being unstable, decay either into leptonically or into hadrons. But considering vector-like electrons which result in stable electrons allows us to probe vector-like leptons using a different approach.

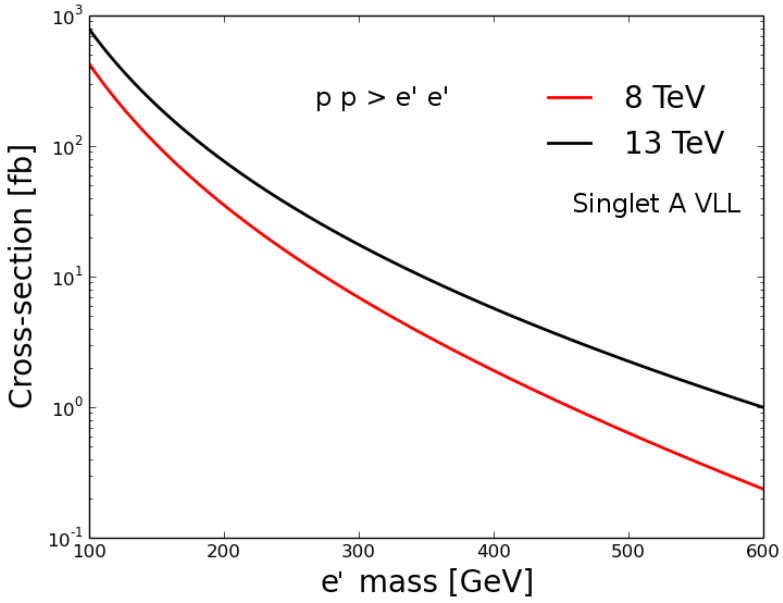

Figure 2.9: Production cross section as a function of mass of vector-like electrons (singlet A VLL model)

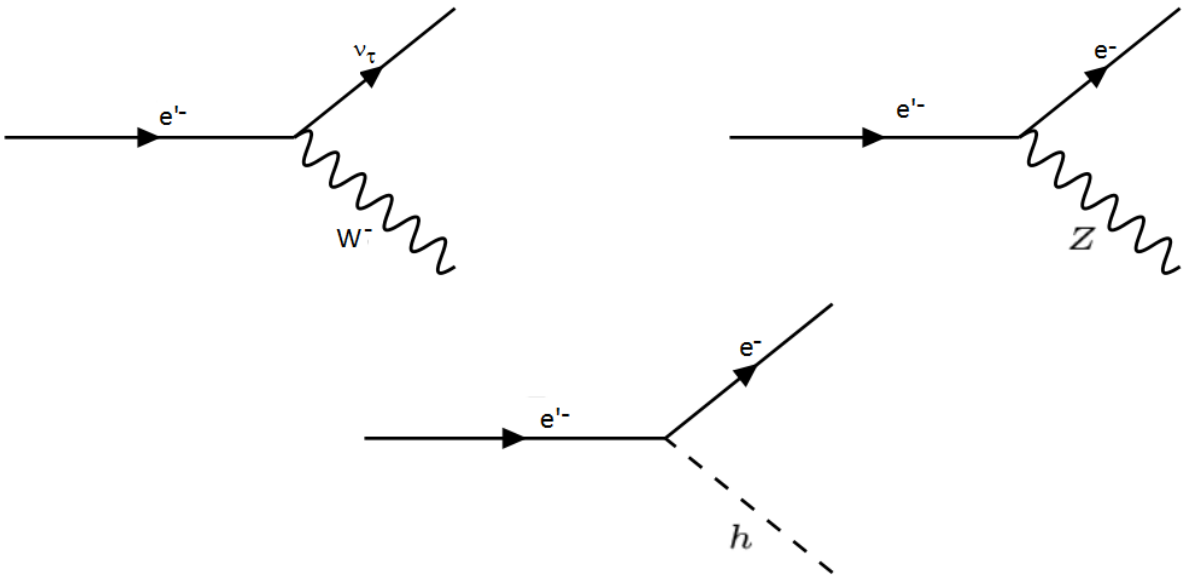

Figure 2.10: Feynman diagrams for the decays of e'^{-} in Singlet A model

In this model, the production is through the pair-production of $e'^{+}e'^{-}$ and the cross section as a function of mass of vector-like electron is shown in Figure 2.9. Here, e'^{-} can decay into $W^{-}\nu_e$, Ze^{-} and He^{-}. The Feynman diagrams corresponding to this decay are given in Figure 2.10. The branching ratio of each of these decays depends on the mass of e' ($m(e')$) and is depicted in Figure 2.11.

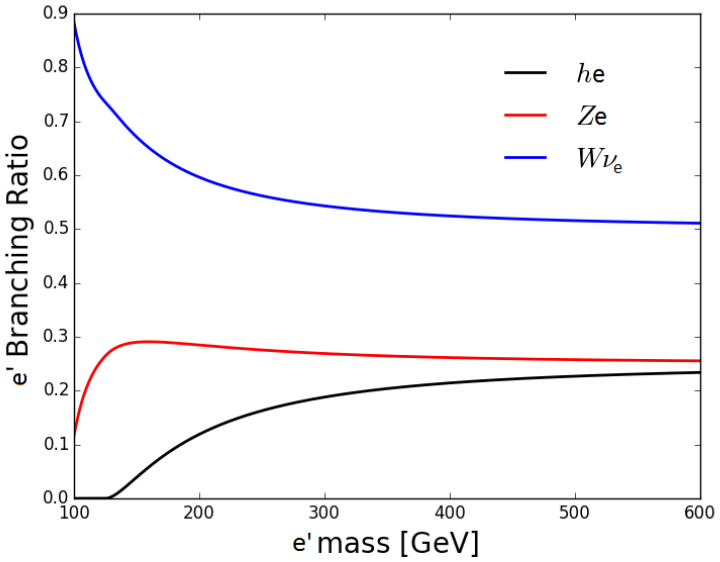

Figure 2.11: Branching ratio of different decay modes of e' as a function of its mass (Singlet A model)

2.4 Previous searches

The L3 collaboration placed a lower bound on additional heavy leptons to be around 100.2 GeV [37]. Recently, the ATLAS collaboration performed a search for heavy lepton resonances decaying into a Z boson and a lepton in a multilepton final state [43]. This search constrained the singlet VLL model and excluded vector-like leptons in the mass range of 114-176 GeV. But there are no such constraints on the doublet VLL model. Given the existing constraints, I consider vector-like leptons with masses more than 100 GeV.

Chapter 3

Analysis strategy

In this thesis, I study pair produced vector-like leptons. The pair production refers to the production of $e'^{+}e'^{-}$ in the singlet A model, $\tau'^{+}\tau'^{-}$ in singlet B model and $\tau'^{+}\tau'^{-}$, $\tau'^{+}\nu'_{\tau}$, $\tau'^{-}\bar{\nu}'_{\tau}$ and $\nu'_{\tau}\bar{\nu}'_{\tau}$ in the doublet model.

When protons collide, different particles are produced and if they are unstable, they decay before reaching the detector. The daughters of these particles may or may not be stable and might result in a series of decays. The particles at the end of this decay chain that interact with the detector are the final state particles. Typically photons, electrons, muons and jets are detected by the detector. If neutrinos are present in the final state, then they contribute to missing transverse energy as they do not interact with the detector. Therefore, we can use any of these as probe to study physics. Vector-like leptons have a rich phenomenology and can be studied using variety of probes including leptons, jets or a combination of both.

I study vector-like leptons using a multilepton final state i.e. final state with three or more charged leptons. For example, Figure 3.1 shows Feynman diagrams for pair production in doublet VLL model and some of the subsequent decays that result in multileptons. This multilepton final state includes hadronic taus. The tau lepton decays before reaching the detector. It either decays leptonically (resulting in electron or muon, and neutrinos) or hadronically (resulting in a jet). When it decays leptonically, the resulting electron or muon are considered in the final state. One advantage of using multileptons is that

the SM cross section to multilepton final state is low, and thus multileptons have low backgrounds compared to jet final state. Multileptons have several parameters that can be used to classify observed excesses. Plus multileptons arise in many different models.

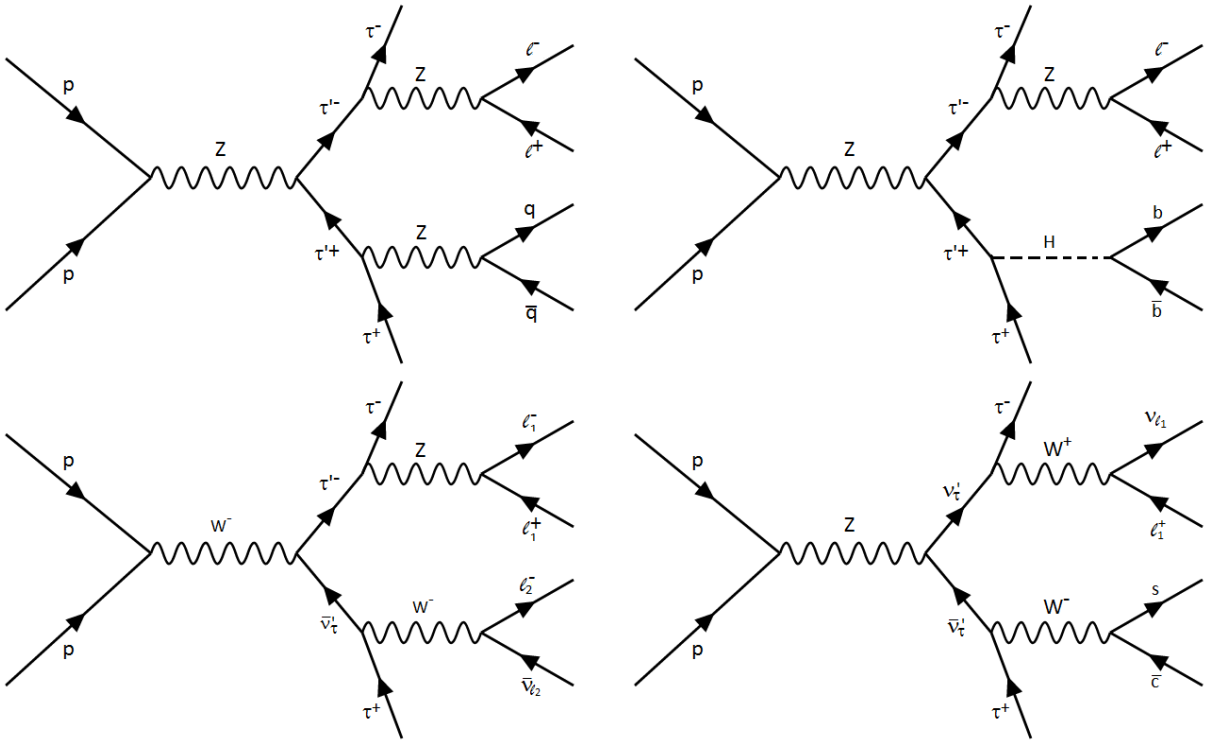

Figure 3.1: Few decays of pair-produced vector-like leptons that give multilepton final state in doublet VLL model. Here, l, l_i (i=1,2) indicate charged leptons (e, μ, τ) where l_i can be leptons of same or different flavor.

To constrain the vector-like leptons in the Run I of the Large Hadron Collider, I use an ATLAS multilepton search [44]. I interpret results from this paper in the context of the doublet VLL model and the singlet A model. The constraints for these models from this interpretation are presented in chapter 5. The interpretation for the singlet B model is provided elsewhere in Ref. [41] and the authors show that a luminosity of 20.3 fb^{-1} used in Ref. [44] is not enough to constrain this model. Even in the most optimistic scenario, a luminosity of at least 350 fb^{-1} is necessary to constrain the singlet B model in Run I of the Large Hadron Collider.

So far, there are no constraints on the vector-like lepton model from Run II of LHC. Hence, I devise a strategy to effectively search for these vector-like leptons using a mul-

tilepton final state. While doing so, it is important to note that some Standard Model processes can also result in multiple leptons in the final state. For example, consider WZ production ($WZ \rightarrow lll\nu$). Such SM processes are referred to as background (as compared to the VLL signal). The important background processes for multileptons are WZ, ZZ, $t\bar{t}W$, $t\bar{t}Z$, Z/γ^*+jets and $t\bar{t}$+jets.

I consider different signal regions based on selection cuts on various kinematic variables. Therefore, an important component of the analysis is to estimate these background processes and devise search regions in order to optimize signal to background ratio. The doublet VLL model is the richest model among the different VLL models that I considered so far. Upon comparing Figures 2.2, 2.6 and 2.9, we see that the production cross section in the doublet VLL model is atleast an order of magnitude higher than the singlet models. This implies that we are more sensitive to the doublet VLL model than the singlet models at the LHC. Therefore for Run II analysis, I optimize my search for the vector-like leptons in the doublet VLL model only.

Chapter 4

Simulation of signal and background samples

There are three steps involved in the Monte Carlo (MC) simulation of collision events. They are listed below.

1. *Event generation*: A MC generator is a piece of software that calculates cross sections and kinematics for a specified process. It simulates the hard scatterings in proton-proton collision events at the Large Hadron Collider. For my analysis, I use MadGraph 5 v2.1.0 [45] which is a generic Monte Carlo generator. In general, MadGraph provides several options and handles to generate specific processes. For example, one can generate a process involving selected decays such as $t\bar{t} \rightarrow W^{+}bW^{-}\bar{b} \rightarrow c\bar{s}b\mu^{-}\bar{\nu}_{\mu}\bar{b}$. Also, one can specify kinematic cuts on generated objects such as leptons, photons and jets. In addition, specific Feynman diagrams contributing to a process can be excluded.

2. *Hadronization*: Free quarks and gluons do not exist in nature, they hadronize. Quarks (or gluons) produce one or more hadrons such that the final result is colorless. The resultant hadrons carry parent quark's (or gluon's) momentum and hence are typically collimated. We cluster these hadrons using particular algorithms [46–51] into objects called as jets. A jet has a well defined four momentum which correlates tightly with the four momentum of the initial quark (or gluon). The exact physics of

hadronization is not well understood but there are models predicting the same [52].

I use PYTHIA v8.186 [53] for the hadronization of the output of the generator. PYTHIA 8 can not only generate Monte Carlo events but also hadronize the MC events simulated by other generators (like MADGRAPH in my case).

3. *Detector simulation*: After simulating the proton-proton collision event, we need to simulate the detector effects. When a particle passes through matter, it interacts with it. For example, a charged particle like electron interacts with the detector through ionization, bremsstrahlung, Cherenkov radiation. A photon interacts via photoelectric effect or pair production. Hadrons interact with the detector through nuclear interactions. All these detector effects on the particles generated in a collision event need to be taken into account. The ATLAS and CMS experiments have proprietary software based on GEANT [54] to accurately simulate the detector interaction with the generated particles. Here, I use parametrization defined by the ATLAS experiment to acess the detector effects on generated leptons where jets are considered, they are reconstructed using generator level information using the anti-k_t jet clustering algorithm [51] in the FastJet [55] package. I use the implementation of Fastjet within the DELPHES v3.1.2 [56] framework.

All the signal and background samples used for this analysis follow the above three steps: event generation in MADGRAPH, hadronization in PYTHIA and detector simulation in DELPHES. Detailed description of the signal and background samples is given in the following sections.

4.1 Signal samples

The doublet VLL model and the singlet A model were explored at 8 TeV and thus the appropriate signal samples were generated as described below. At 13 TeV, only the doublet VLL model was studied and signal samples pertaining to this model were generated.

4.1.1 Model implementation

MadGraph provides instructions to implement a new model in its framework. Some models are already available in MadGraph such as the Standard Model.

Doublet VLL model

Model implementation for the doublet VLL model was done with the help of Stephen Martin and Nilanjana Kumar [41]. They implemented this model in FeynRules v2.0.25 [57] which allows one to start from the Lagrangian of a model and obtain the interaction vertices and their couplings. The output generated by FeynRules contained all the information about the particles in the model including their interactions, couplings, decays and branching ratios. I was provided with this output and I imported it into MadGraph framework. Upon doing this, MadGraph allowed me to generate events for the doublet VLL model. For the Run I analysis, I generated pair-produced $\tau'^{+}\tau'^{-}$ with m(τ') = 150, 200, 250, 300, 400 and 500 GeV. I generated the pair-produced vector-like taus with m(τ') in the range of 280-500 GeV for the Run II analysis. The cross section at 8 TeV and the cross section at 13 TeV is listed in Table 4.1.

$m(\tau')$=$m(\nu'_\tau)$ (GeV)	8 TeV cross section (fb)	13 TeV cross section (fb)
150	245.8	-
200	81.17	-
250	32.5	-
280	-	50.1
300	14.9	40
350	-	20
400	3.846	10.42
425	-	10
450	-	8
475	-	7
500	1.242	5.5

Table 4.1: The mass of vector-like leptons for different signal samples and the corresponding production cross section in the doublet VLL model at 8 TeV and 13 TeV

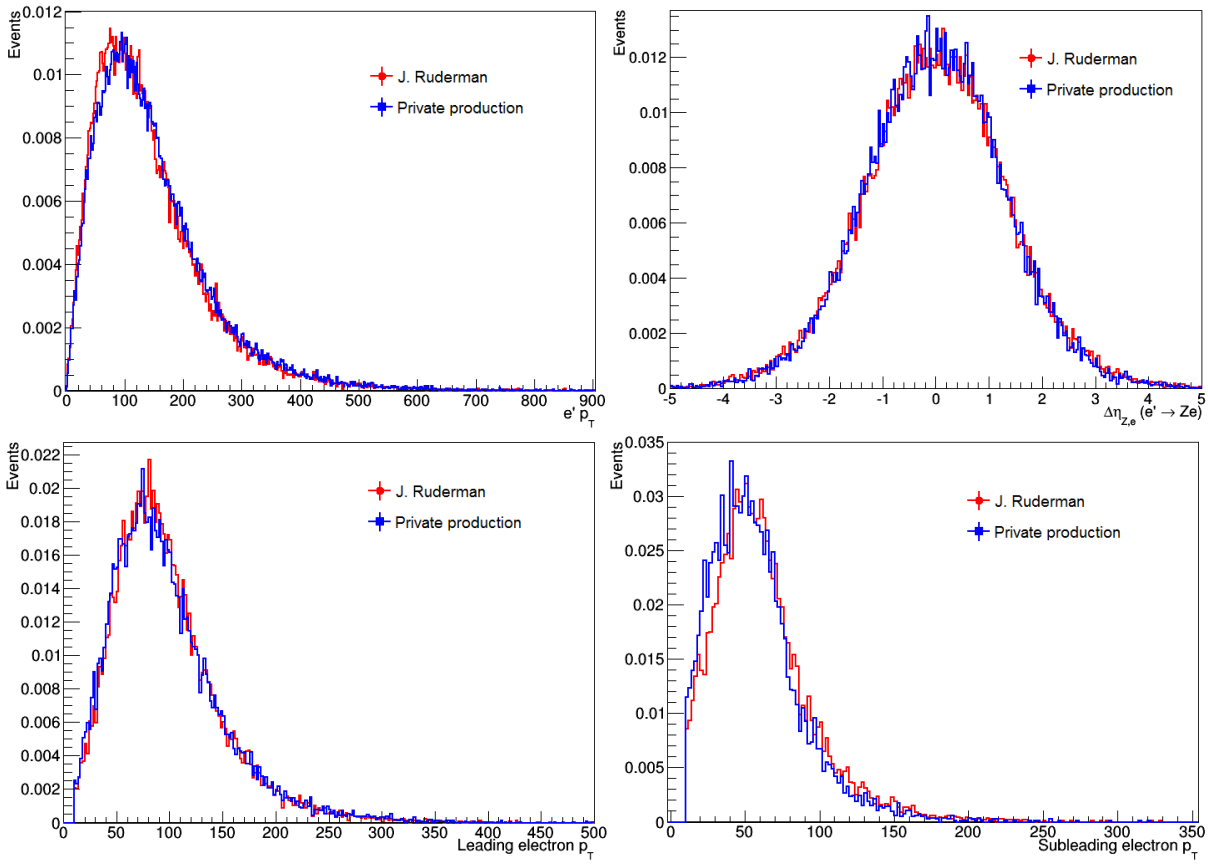

Figure 4.1: Comparison plots between my implementation (labeled Private production) and the pre-existing signal sample (labeled J. Ruderman) for m(e')=100 GeV. The top left panel shows the distribution of e' p_T, the top right plot is the $\Delta\eta$ between Z, e which result from decay of e', the bottom left plot is the p_T distribution of leading electron in the sample and the bottom right plot shows the p_T distribution of subleading electron in the event. All these plots show reasonable agreement of the kinematic variables with the available sample.

Singlet A model

Simulation samples for this model at the generator level were available for two mass values of e' [58]. Based on these samples, I implemented this model in the MadGraph (v2.1.0) framework. [1]

I validated my implementation of the model by comparing some kinematic distributions with the previous samples. I reproduced distributions such as the transverse momentum, p_T, of different particles such as e', leading lepton (the lepton with highest

[1] In my implementation, I assumed the Standard Model like couplings for vector-like electrons.

p_T), subleading lepton (the lepton with second highest p_T) and I also compared the angular distribution between Z and the electron which decay from an e'. Figure 4.1 shows some of the comparison plots between the sample I generated and the existing sample for $m(e')$=100 GeV.

Though Figure 4.1 shows consistency in both the generations, some discrepencies remain which can be partially related to differences between MadGraph 4 v4.5.2 and MadGraph 5 v.2.1.0. An important difference could be that different couplings were implemented in both the generations. This difference would be pursued during further studies.

$m(e')$ (GeV)	Cross section (fb)
100	427.966
200	35.3255
300	6.9138
400	1.90869
500	0.634002

Table 4.2: The mass of vector-like electron for different signal samples and the corresponding production cross section in the singlet A VLL model at 8 TeV

I generated signal samples for vector-like electrons of masses 100, 200, 300, 400 and 500 GeV. The cross section for these mass points are given in Table 4.2.

4.2 SM Background samples

I generated background samples for LHC Run II analysis at a center of mass energy of 13 TeV. The SM background processes that give multileptons are WZ, ZZ, $t\bar{t}V$ (here $V = W/Z$), $Drell - Yan$+jets and $t\bar{t}$+jets. In all these processes, Z represents Z boson and the virtual photon, γ^*. Some important details of the generation of these samples is summarized in Table 4.3.

Background sample	Cuts	Cross section (pb)	Branching ratio	Number of events	Luminosity (fb^{-1})
$WZ \to lll\nu$	$m_{ll} > 4$ GeV	4.4	1.0	50,000	11.4
$ZZ \to llll$	$m_{ll} > 4$ GeV	1.2	1.0	50,000	41.7
$t\bar{t}W(\to lll\nu\nu\nu b\bar{b})$ $t\bar{t}Z(\to llll\nu\nu b\bar{b})$	-	0.17	1	950,000	5588
$Z/\gamma^*(\to ll)$+jets	$m_{ll} \geq 10$ GeV	24635	1	100,000	0.004
$t\bar{t}(\to ll\nu\nu b\bar{b})$+jets	-	831.8	0.106	4,000,000	45

Table 4.3: List of all the SM background processes with their cross section (pb), number of events and Luminosity (fb^{-1}) specified. Here, Z=Z/γ^* and $l = e/\mu/\tau$. I am predicting exclusion limits for a luminosity of 20 fb^{-1}.

Chapter 5

Analysis for LHC Run I data

LHC Run I comprises of proton-proton collision data recorded at center of mass energy of 7 TeV and 8 TeV. For my analysis purposes, I consider only 8 TeV data as it corresponds to a luminosity of 20.3 fb^{-1} whereas the 7 TeV data corresponds to a luminosity of around 5 fb^{-1}.

5.1 Model testing using an ATLAS 8 TeV search

The ATLAS experiment has performed a model independent multilepton search using pp collisions at $\sqrt{s} = 8\ TeV$ [44]. In this paper, ATLAS provides a prescription to constrain any beyond Standard Model physics that results in multileptons. Here, I describe how I use this prescription to constrain vector-like leptons.

Results in Ref. [44] are presented in terms of visible cross section, σ_{vis}. These can be inverted to obtain a 95% CL [59, 60] upper limit on the number of events, N_{95}, using $N_{95}=\mathscr{L}\cdot\sigma_{vis}$. If a model predicts more number of events than N_{95} for the same luminosity, then it is excluded.

Thus for vector-like lepton models, we need to calculate the number of signal events, N_{sig} and compare it with N_{95}. Alternatively, I can convert N_{sig} into visible cross section and compare against the upper limit on σ_{vis} from Ref. [44]. I present results for the vector-like lepton models in terms of σ_{vis}. In order to calculate the expected σ_{vis} from

the model, I use following relations.

$$N_{sig} = \mathscr{L} * \sigma * B * A * \epsilon \tag{5.1}$$

$$\sigma_{vis} = \frac{N_{sig}}{\mathscr{L}} \tag{5.2}$$

Equation 5.1 relates the production cross section (σ) to the number of signal events (N_{sig}) where $\mathscr{L}$ is the luminosity, B is the branching ratio, A is the acceptance and ϵ in the efficiency. Here, the luminosity is same as the original result i.e. $\mathscr{L}$=20.3 fb^{-1}. The cross section for the pair-produced vector like leptons is given by the model. For example, cross section of $\tau'^{+}\tau'^{-}$ at m(τ')=150 GeV in the doublet VLL model is 245.8 fb. The cross sections of the signal samples used for the doublet VLL model is listed in Table 4.1 and for the singlet A model are listed in Table 4.2. During the generation of samples, if the vector-like leptons or the SM bosons resulting from their decay are forced to decay into leptons, then the appropriate branching ratio needs to be taken into account. For example, consider the following production for m(τ')=150 GeV in the doublet VLL model.

$$p\ p \ \rightarrow \ \tau'^{+}\tau'^{-} \ \rightarrow \ Z\tau^{+}H\tau^{-} \ \rightarrow \ l^{+}l^{-}\tau^{+}H\tau^{-}$$

Here, the τ'^{+} is forced to decay to $Z\tau^{+}$, τ'^{-} decays to $H\tau^{-}$ and the resultant Z decays leptonically. The branching ratio of each of these decays is $B(\tau'^{+} \rightarrow Z\tau^{+})$=0.87, $B(\tau'^{-} \rightarrow H\tau^{-})$=0.13 and $B(Z \rightarrow l^{+}l^{-})$=0.10099 where $l = e/\mu/\tau$. The total branching ratio for the generated process is given by multiplying these individual branching ratio. Therefore, the total branching ratio for this generation is 0.0114. For illustration, consider the branching ratio of pair-produced vector-like electrons to 3 or more leptons in the singlet A model. Figure 5.1 depicts this branching ratio as a function of vector-like electron mass.

The $A * \epsilon$ in equation 5.1 is experimental in nature. The acceptance is a measure of the number of events that satisfy our event selection requirements whereas the efficiency refers to the effectiveness of detecting an event within the fiducial volume of the detector. Therefore, this can only be ascertained by simulation of the signal sample and applying precisely the same selections as in the paper. The exact event selection is described in the next section.

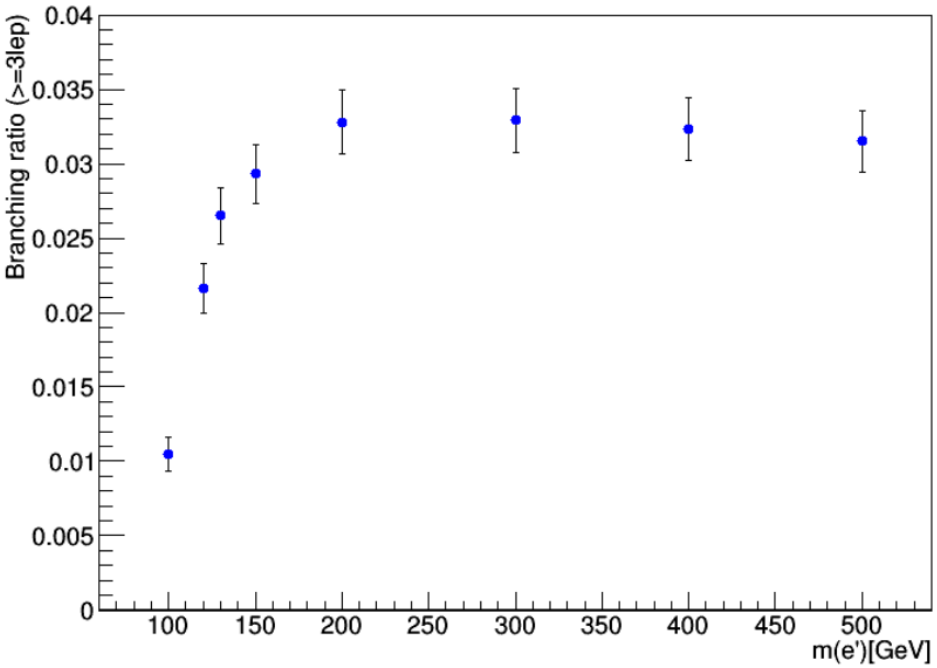

Figure 5.1: Branching ratio to trileptons for pair-produced vector-like electrons in the singlet A model as a function of their mass.

5.2 Event selection

I select events using generator-level information. The output of the detector (detector-level) is different from generator-level information due to the efficiency of reconstructing objects from detector information and the resolution of those measured quantities. The correction factor to go from generator-level to detector-level is provided for individual leptons in Ref. [44] based on their flavor, position and momentum. This correction is measured using a WZ simulated sample.

Here, the electrons and muons are selected if their transverse momentum, p_T, is above 10 GeV and their pseudorapidity, $|\eta|$, falls within the fiducial volume of the detector (see Table 5.1). For hadronically decaying taus, τ_{had}, the selection cuts are placed on visible transverse momentum, p_T^{vis}, and visible pseudo-rapidity, $|\eta^{vis}|$. Here, visible indicates that the resultant four-momentum from the daughters of τ_{had} that interact with the detector material. For example, if $\tau^- \rightarrow \pi^-\nu_\tau$ then the $p_T^{vis} = p_T$ of π^- (neutrino is ignored as it does not interact with the ATLAS detector). To obtain isolated electrons and muons, we consider a cone of ΔR=0.3 around the lepton's direction and sum the magnitude of

S.No.	Event selection cuts
1	Electron: p_T>10 GeV and 1.52<$\|\eta\|$<2.47 or $\|\eta\|$<1.37
2	Muon: p_T>10 GeV and $\|\eta\|$<2.5
3	Hadronically decaying tau: p_T^{vis}>15 GeV and $\|\eta^{vis}\|$<2.5
4	Isolation cuts: $\|\Sigma p_T^{iso}\|/p_T$<0.15 and $\|\Sigma E_T^{iso}\|/p_T$ within cone of ΔR=0.3 for both electrons and muons.
5	Jets: p_T>30 GeV and $\|\eta\|$<4.9
6	Overlap removal: Muons with jets inside ΔR<0.4 are rejected. If an electron or τ_{had} has a jet within ΔR<0.2, then the jet is neglected. If jet and electron's separation satisfies 0.2<ΔR<0.4, then electron is neglected. Electrons having muons withinΔR<0.1 are ignored. Also, if two electrons are within ΔR<0.1, then the electron with lower p_T is rejected.

Table 5.1: Event selection for the 8 TeV analysis

p_T of charged particles whose p_T>1 GeV within this cone. An upper bound is placed on the ratio of this sum to the lepton p_T. A similar upper bound is placed on the ratio of sum of transverse energy, E_T, of visible particles (except muons) within the same cone to the lepton p_T. The second isolation requirement includes the neutral particles unlike the first isolation requirement. We also place minimum p_T requirements on jets to be 30 GeV and have pseudo-rapidity, $|\eta|$, less than 4.9. To ensure that the isolated leptons are not a part of a jet, we remove the overlap between jets and the selected leptons as mentioned in Table 5.1. The event selections that I used in my analysis are summarized in Table 5.1.

5.2.1 Event efficiency

The event efficiency is refers to the efficiency of detecting an event within the fiducial volume of the detector. Here, the fiducial volume of the detector refers to the active parts of the detector within the acceptance region. The total efficiency of a multilepton event depends on the individual lepton efficiencies. These individual lepton efficiences are provided in the ATLAS paper.

For such an event with exactly three leptons, the total efficiency of the event is the product of the three individual lepton efficiencies. If l_1, l_2 and l_3 are the only three

leptons in the event, then efficiency of total event is $\epsilon_1\epsilon_2\epsilon_3$ where ϵ_i is the efficiency of l_i. For an event with four leptons (l_1, l_2, l_3, l_4), consider the combination of three leptons, for example, $l_1l_2l_4$, the efficiency for this combination is given by $\epsilon_1\epsilon_2\epsilon_4(1-\epsilon_3)$. Here $(1-\epsilon_3)$ terms takes into account the inefficiency of detecting the 3rd lepton. Similarly, a combination of $l_2l_3l_4$ has an efficiency of $\epsilon_2\epsilon_3\epsilon_4(1-\epsilon_1)$. We need to consider all such trilepton combinations in order to calculate the four lepton event efficiency. This procedure can be extended to any number of leptons that might be in an event. A detailed description can be found in Ref. [61].

5.2.2 Signal regions

Events satisfying the above mentioned event selection criteria are divided into two channels. The first channel is when the event has three or more electrons or muons which is referred to as $\geq$3e/μ channel. The second channel consists of the events which have exactly two electrons or muons and atleast one hadronically decaying tau. The second channel is referred to as =2e/μ+$\geq$1τ_{had} and this channel is orthogonal to $\geq$3e/μ channel.

Each of these channels is further divided into three categories: "on-Z", "off-Z, OSSF" and "off-Z, no OSSF". The first category refers to the events in which we have atleast one opposite sign same flavor (OSSF) leptons that has invariant mass in the range 81-101 GeV (20 GeV mass window around Z boson mass). The events which have an OSSF lepton pair but with invariant mass outside this mass range belong to the second category, "off-Z, OSSF". The third category, "off-Z, no OSSF" comprises of events that have no OSSF lepton pair. For this categorization, only the three leading leptons in >=3e/μ channel are considered and in the =2e/μ+$\geq$1τ_{had} channel, we consider the two light leptons and the leading τ_{had} (one with the highest p_T).

We categorize events in this fashion in order to distinguish events with a Z boson and the events without a Z boson. For example, WZ background would predominantly contribute to the "on-Z" channel where as $t\bar{t}$+jets contributes to the "off-Z" channel. Similarly, the signal events may or may not comtain a Z boson and undergo similar classification. It is important to note that these three categories are mutually exclusive.

Signal Region Number	Kinematic Variable Cut
0	all inclusive
1	H_T^{lep} >200 GeV
2	H_T^{lep} >500 GeV
3	H_T^{lep} >800 GeV
4	H_T^{jets} <150 GeV
5	H_T^{jets} <150 GeV, E_T^{miss} > 100 GeV
6	H_T^{jets} <150 GeV, E_T^{miss} > 200 GeV
7	H_T^{jets} <150 GeV, E_T^{miss} > 300 GeV
8	H_T^{jets} ≥150 GeV
9	H_T^{jets} ≥150 GeV, E_T^{miss} > 100 GeV
10	H_T^{jets} ≥150 GeV, E_T^{miss} > 200 GeV
11	H_T^{jets} ≥150 GeV, E_T^{miss} > 300 GeV
12	m_{eff} >600 GeV
13	m_{eff} >1000 GeV
14	m_{eff} >1500 GeV
15	E_T^{miss} ≥100 GeV
16	m_{eff} >600 GeV, E_T^{miss} ≥100 GeV
17	m_{eff} >1200 GeV, E_T^{miss} ≥100 GeV

Table 5.2: Different signal regions based on the kinematic variables used for the interpretation. Signal region number 0 corresponds to an all inclusive channel (with no cuts on E_T^{miss}, H_T^{lep}, H_T^{jets} and m_{eff}). For full signal regions, refer Table 1 in Ref. [44].

Therefore, we can perform analysis separately in these categories and statistically combine them to obtain a better exclusion limit.

After this, the events are divided into different signal regions based on the cuts on different kinematic variables, as shown in Table 5.2. H_T^{lep} is calculated by the scalar sum of the p_T (or p_T^{vis} for τ_{had}) of leptons that define the multilepton event. H_T^{jets} is obtained by the scalar sum of p_T of all the selected jets in the event. E_T^{miss} is defined as the vector sum of all the stable, invisible particles at the generator level. In my analysis, only the Standard Model neutrinos contribute to E_T^{miss} and hence, vector sum of neutrinos in the event is equal to E_T^{miss}. The kinematic variable effective mass, m_{eff}, is the sum of H_T^{lep}, H_T^{jets} and E_T^{miss}. I used signal regions based on these variables for my analysis. For detailed list of all signal regions, refer Table 1 in Ref. [44].

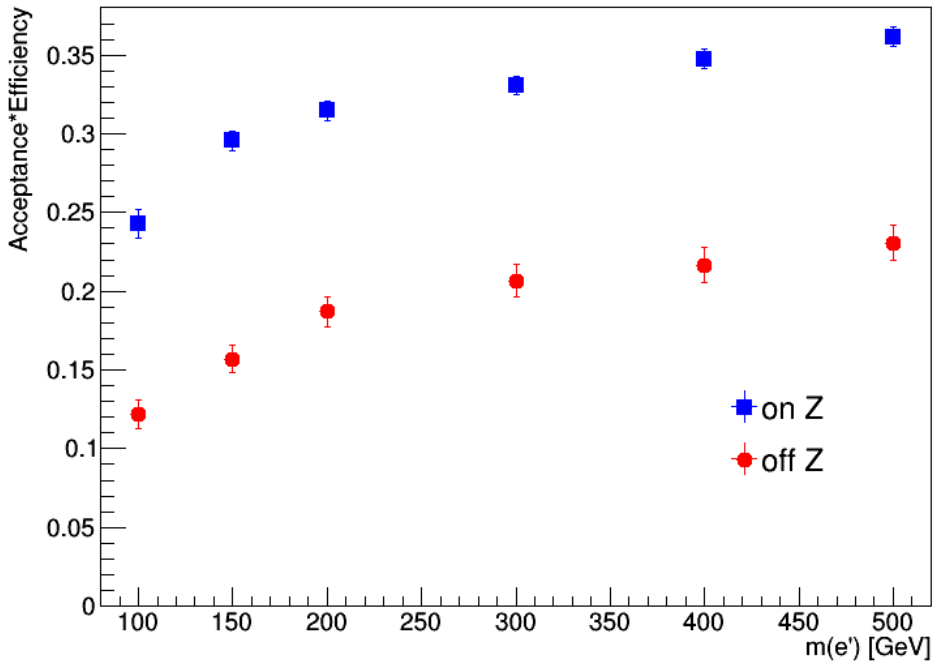

Figure 5.2: Acceptance times efficiency as a function of vector-like electron mass for singlet A VLL model. The plot is for an all inclusive signal region for $\geq 3e/\mu$ channel.

The acceptance in each signal region is given by the ratio of the number of events that satisfy all the selection requirements of particular signal region to the total number of events processed. By multiplying this acceptance with the event efficiency obtained from the earlier calculation, we can obtain the acceptance times efficiency for the signal sample. For example, the acceptance times efficiency as a function of the VLL mass for the singlet A VLL model is given in Figure 5.2.

5.3 Kinematic distributions

Here, I present some distributions for the kinematic distributions such as E_T^{miss}, H_T^{lep}, H_T^{jets} and m_{eff} based on which the signal regions that I use for the analysis are defined. Figure 5.3 gives comparison plots of these kinematic variables for different VLL masses of the doublet model. As the mass of vector-like lepton increases, we see that peak of the distributions shift to the right side. This is because if the mass of the vector-like tau is more, then the resulting leptons will have higher p_T which in turn shows up as higher E_T^{miss}, H_T^{lep}, H_T^{jets} and m_{eff}. These distributions for the singlet A VLL model for

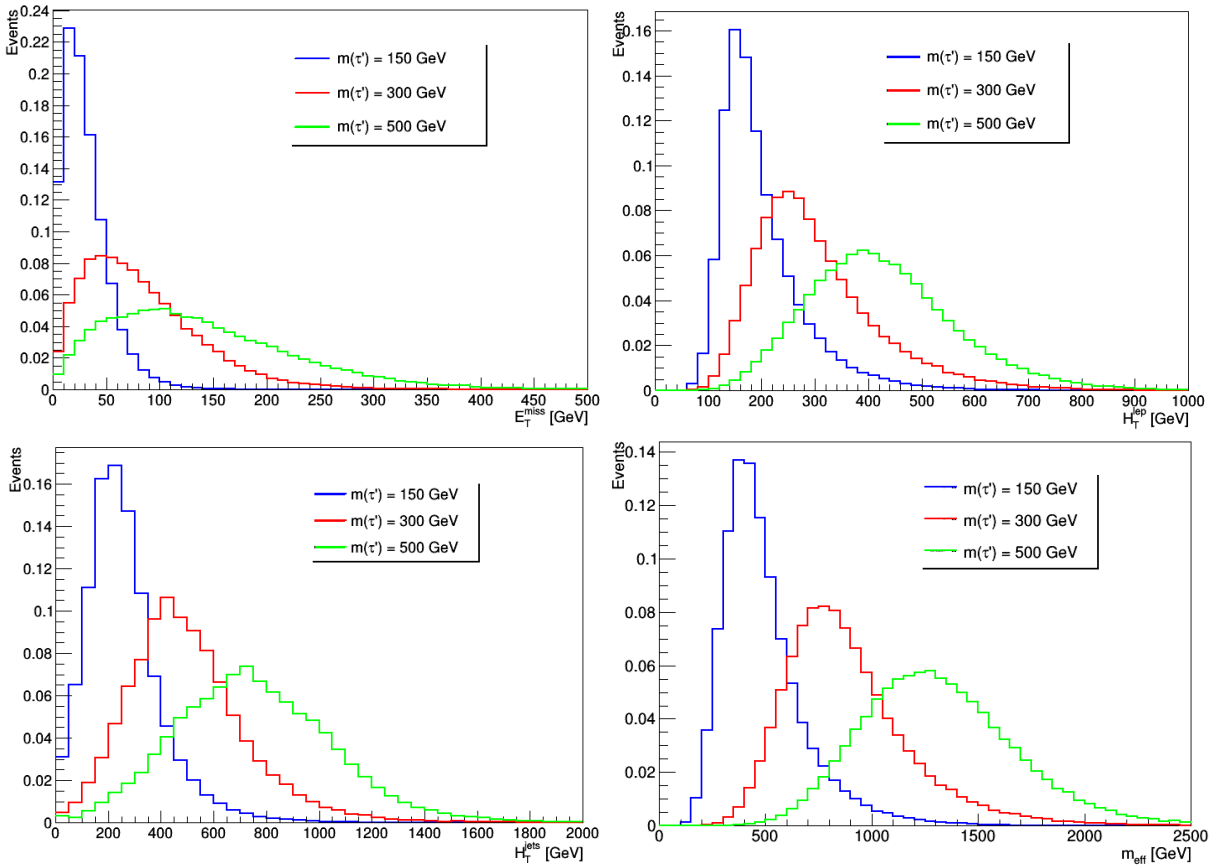

Figure 5.3: Comparison plots of different kinematic variables like E_T^{miss}, H_T^{lep}, H_T^{jets} and m_{eff} for different masses of vector-like electrons in the doublet VLL model. Here, I consider m(τ')=150, 300 and 500 GeV.

m(e')=100, 300 and 500 GeV are shown in Figure 5.4.

5.4 Interpretation of the results

Using equation 5.1, we obtain the expected visible cross section for the VLL model which we can compare against the measured σ_{vis} given in Ref. [44].

5.4.1 Doublet model

The signal sample for this model is pair-produced $\tau'^{+}\tau'^{-}$ where one of the τ' is forced to decay into $Z\tau$. One Z in the decay chain always decays leptonically. So the allowed decay chains are $Z\tau^{+}Z\tau^{-}$, $Z\tau^{+}H\tau^{-}$ and $H\tau^{+}Z\tau^{-}$ where one Z is forced to decay leptonically. The corresponding branching ratio is taken into consideration while calculating

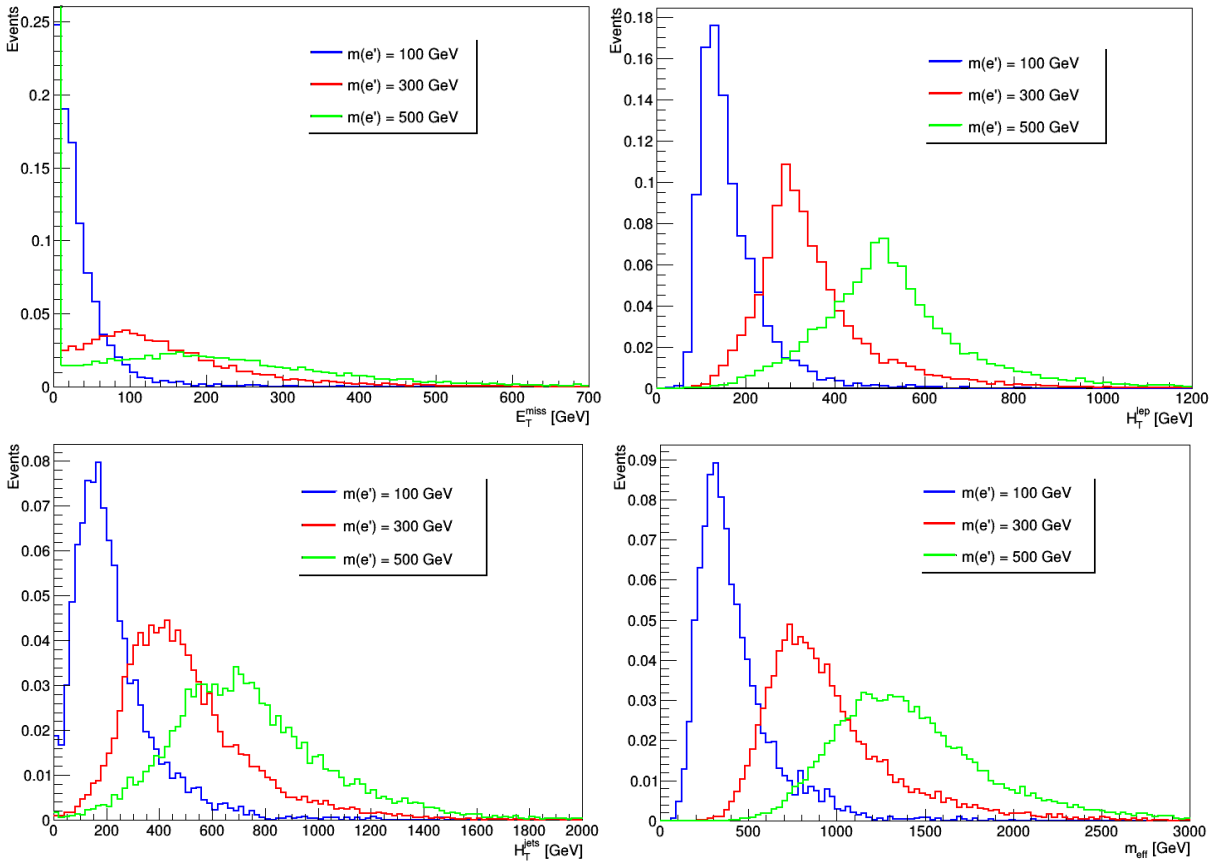

Figure 5.4: Comparison plots of different kinematic variables like E_T^{miss}, H_T^{lep}, H_T^{jets} and m_{eff} for different masses of vector-like electrons in the singlet A model. Here, I consider m(e')=100, 300 and 500 GeV.

the exclusion limit.

By using =2e/μ+$\geq$1τ_{had}, off-Z OSSF channel and signal region $H_T^{lep} \geq 200$ GeV, I rule out vector-like leptons with m(τ')<280 GeV. Figure 5.5 shows the comparison between the expected and measured σ_{vis} for this signal region.

5.4.2 Singlet B model

I have not probed this model at LHC using the Run I data, but I quote the result from reference [41] for completeness. Figure 2.6 shows that the production cross section in this model is very low at a center of mass energy of 8 TeV. As a result of which, we are not sensitive to this model with a luminosity of 20.3 fb^{-1}. More data, typically of order of 100 fb^{-1}, is necessary to discover or constrain this particular model [41].

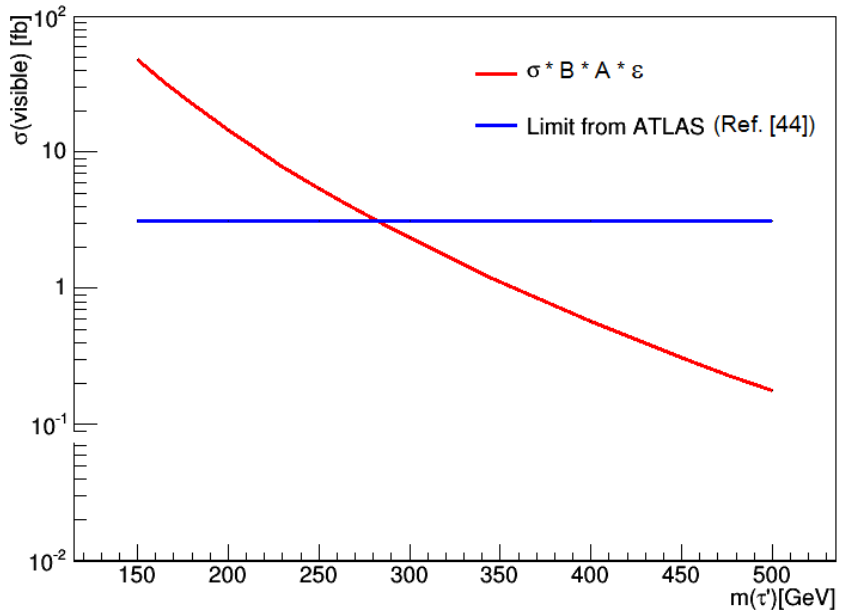

Figure 5.5: Observed and expected 95% CL upper limit on the visible cross section in =2e/μ+$\geq$1τ_{had}, off-Z OSSF channel with $H_T^{lep} \geq 200$ GeV

5.4.3 Singlet A model

In the singlet model, I pair-produce vector-like electrons ($e'^+e'^-$) and force one of them to decay to Ze. Therefore, the allowed decay modes are Ze^+Ze^-, Ze^+He^-, $Ze^+W^-\nu_e$ and $W^+\bar{\nu_e}Ze^-$.The corresponding branching ratio for this generation is also taken into consideration.

Upon calculating the exclusion limit for different signal regions, the most constrained region is $\geq 3e/\mu$, off-Z OSSF channel with $m_{eff} \geq 600$ GeV. The exclusion contour for the corresponding signal region is given in Figure 5.6. Therefore, vector-like leptons in the singlet A VLL model with masses below 150 GeV are excluded.

5.4.4 Summary

I constrained the vector-like lepton models in the Run I of the Large Hadron Collider. The 95% confidence level lower bound on the masses of different vector-like leptons is summarized in Table 5.3.

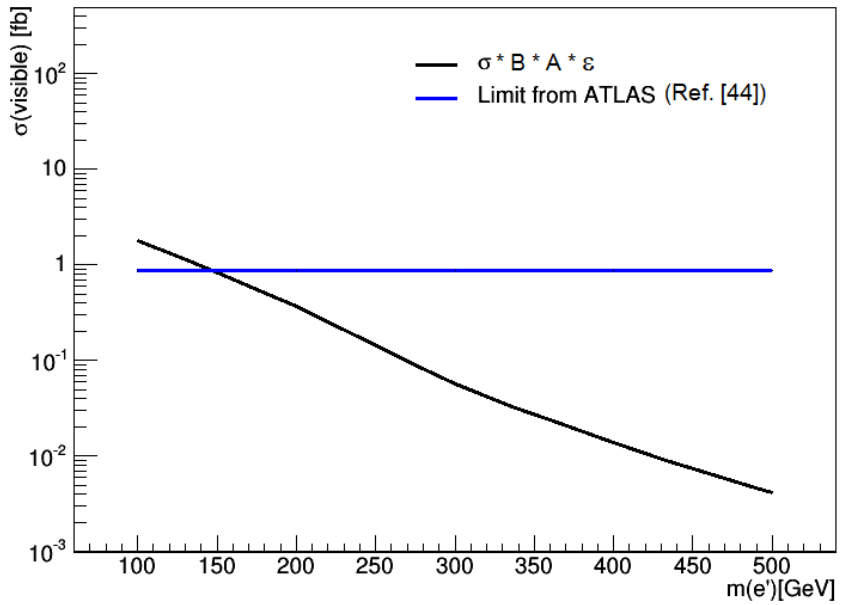

Figure 5.6: Observed and expected 95% CL upper limit on the visible cross section in $\geq 3e\mu$, off-Z OSSF channel with $m_{eff} \geq 600$ GeV

Model	Excluded at 95% CL
Doublet VLL	m(τ')<280 GeV
Singlet B VLL	No exclusion
Singlet A VLL	m(e')<150 GeV

Table 5.3: The 95% Confidence Level (CL) exclusion limit on vector-like leptons in different VLL models.

From Section 2.4, we saw that Ref. [43] excluded vector-like leptons in the singlet model with masses in the range of 114-176 GeV. The lower bound from my analysis is around 150 GeV which is comparable to this result. Analysis designed for specific models typically place stronger cosntraints on the model as compared to model independent analysis. But, as can be seen by comparing these two numbers, the model independent analysis does provide a good estimate of the constraints.

Chapter 6

LHC Run II prospects

I study the prospects of discovering or excluding the vector-like leptons within the doublet model in the Run II of the LHC. The cross section for pair-produced $\tau'\tau'$, $\tau'\nu'_\tau$ and $\nu'_\tau\bar{\nu}'_\tau$ at 13 TeV is shown in figure 2.2. For this analysis, I pair-produced $\tau'^{+}\tau'^{-}$ where one of the τ' is forced to decay to Zτ. This implies that the possible decays are $Z\tau^{+}Z\tau^{-}$ and $Z\tau^{+}H\tau^{-}$ with one of the Z bosons decays leptonically. As the limit from Run I analysis is 280 GeV on vector-like lepton mass, here I consider m(τ')$\geq$280 GeV.

6.1 Event pre-selection

All the selection criteria discussed here are applied at the generator level. Electrons and muons should satisfy p_T > 10 GeV and $|\eta|$ <2.4. Electrons and muons are required to be isolated with Trackiso<0.15. TrackIso is defined as the ratio of the scalar sum p_T of all charged particles with p_T >1 GeV, in a cone of ΔR=0.3 around the lepton to the lepton's p_T. Hadronic taus need to satisfy p_T >20 GeV, $|\eta|$ <2.3 and E_{iso} <2.0. The E_{iso} is defined as the sum of energy of all the particles in a cone of ΔR=5.0 around the lepton direction. For hadronic taus, the isolation is defined as the ratio of sum of energy of all the particles within this cone to the p_T of the tau lepton. The leading lepton p_T in the selected events should at least be 20 GeV. All the selected jets in an event should have p_T>30 GeV and $|\eta|$<2.5. To remove lepton-jet overlap, any jet that comes within ΔR<0.3 of a lepton is vetoed. These selections follow the 8 TeV CMS multilepton paper [66] and

are summarized in Table 6.1.

S.No.	Event selection cuts
1	Electron and muon: p_T >10 GeV and $\|\eta\|$ <2.4
2	Hadronically decaying tau: p_T^{vis} >20 GeV and $\|\eta^{vis}\|$ <2.3
3	Isolation cuts: $\|\Sigma p_T^{iso}\|/p_T$ <0.15 within cone of ΔR=0.3 for both electrons and muons. E_{iso} <2.0 within cone of ΔR=0.5 for hadronic taus.
4	Jets: p_T >30 GeV and $\|\eta\|$ <2.5
5	Overlap removal: If a lepton has a jet within ΔR<0.3, then the jet is rejected.
6	Leading lepton in the event has p_T >25 GeV.

Table 6.1: Event selection for the Run II analysis

In order to incorporate the detector response, I follow the same procedure as in section 5.2.1. Here, I assume that the per-lepton efficiencies at 13 TeV would be comparable to those at 8 TeV. This assumption is not unreasonable as the muon identification efficiency at the CMS and the ATLAS experiments did not change appreciably from Run I to Run II [67–71]. Therefore, I use the same per-lepton efficiencies listed in Ref. [44] for the Run II analysis.

6.2 Background estimation

The Standard Model backgrounds that give multileptons are WZ, ZZ, ttV ($V = W/Z$), $t\bar{t}$, and Z/γ^*+jets. These backgrounds can be broadly classified into two categories as discussed below.

1. *Irreducible backgrounds*: These SM backgrounds give at least three genuine leptons in the final state. Backgrounds like WZ, ZZ, ttV belong to this category. They are estimated using the simulated Monte Carlo samples. I compare to results shown in Ref. [72] and assign uncertainties as follows. I assign 10% uncertainty on WZ background and 38% on ZZ. These uncertainties are conservative, and in practice could be reduced leading to stronger constraints.

2. *Misidentified lepton backgrounds*: Backgrounds such as $t\bar{t}$ and Z/γ^*+jets only give two genuine leptons in the final state. The third lepton might arise from a jet and

can be misidentified as a genuine lepton. For example, in $t\bar{t}$, two W bosons result in two leptons and a semi-leptonic decay of a hadron from one of the b jets can give the third lepton. These backgrounds cannot be accounted for directly from the generator-level information as the probability of a jet faking a lepton depends on its properties and its interaction with the detector material.[1] I estimate the $t\bar{t}$ background using the simulated sample of luminosity of 45 fb^{-1}. In order to be conservative, I assign 100% uncertainty on my $t\bar{t}$ estimate.

In a recent CMS multilepton result [72], the contribution of Z/γ^*+jets was comparable to that of $t\bar{t}$ for particular set of selections. Here, I assume that the Z/γ^*+jets background estimate is same as $t\bar{t}$+jets. Typically, Drell-Yan events will have less E_T^{miss} and jet activity compared to $t\bar{t}$. Thus my approach is conservative while searching for my signal. I assign 100% uncertainty on the Drell-Yan events to account for any differences in the event topology from the $t\bar{t}$.

6.3 Signal regions

The event classification has a similar flow as in the Run I analysis. I first classify the events into two mutually-exclusive channels, $\geq 3e/\mu$ and $=2e/\mu+ \geq 1\tau_{had}$. The former channel comprises of the events with at least three or more electrons and muons. The events which have exactly two electrons or muons and at least one hadronically decaying tau fall into the latter channel. I further categorize events in each channel into "onZ" and "offZ" depending on whether they have an OSSF pair with invariant mass 91$\pm$10 GeV or not.

Figure 6.1 shows the distributions of kinematic variables such as number of leptons (e/μ), number of hadronic taus and the number of jets for m(τ')=300, 400 and 500 GeV. We observe that the number of leptons and jets peak at the same value for different masses of τ'. Similar distributions for kinematic variables such as E_T^{miss}, H_T^{lep}, H_T^{jets} and m_{eff} for $\geq 3e/\mu$ channel are depicted in figure 6.2. However, the peaks in the kinematic distributions in figure 6.2 shift to higher values as m(τ') increases. This is expected because if

[1] These backgrounds are not even considered in some analysis, for example Ref. [41].

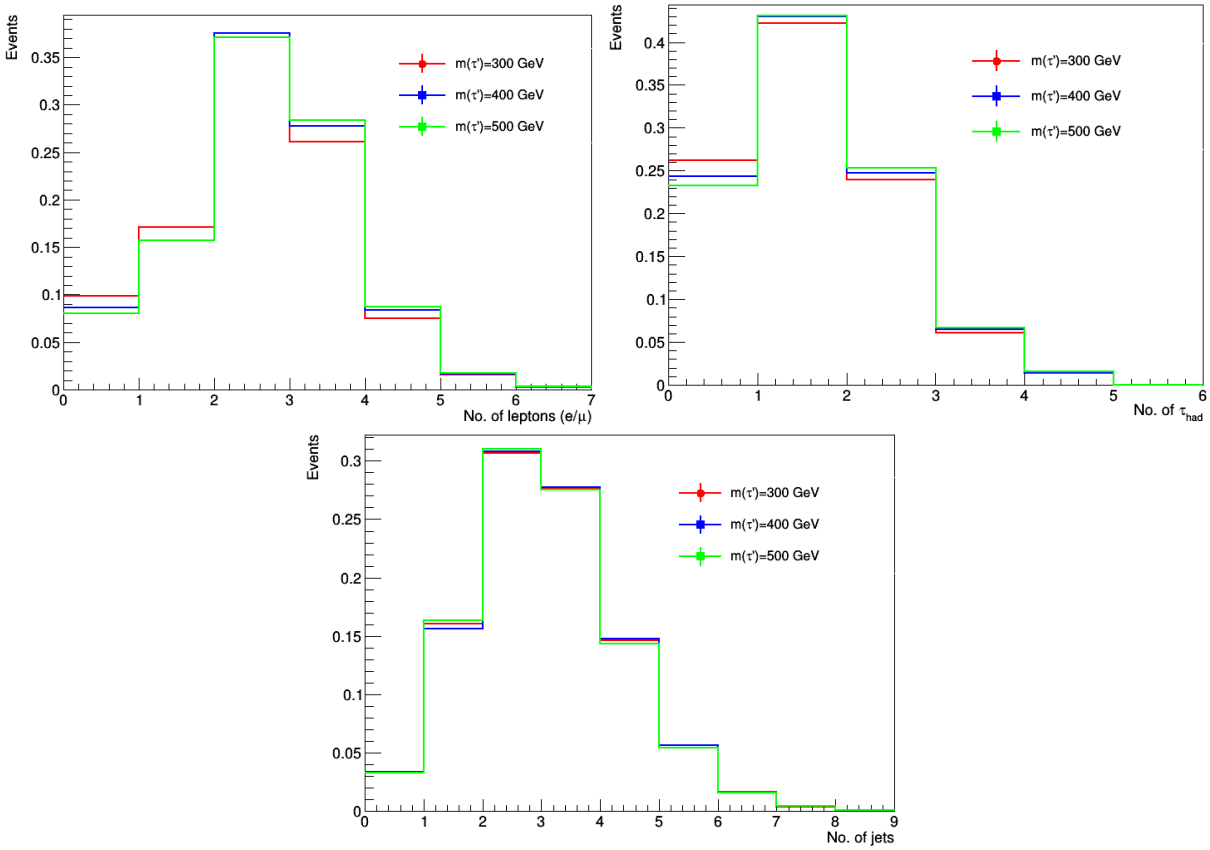

Figure 6.1: The top left panel shows the number of leptons (e/μ), the top right plot shows the number of hadronic taus and the bottom panel displays the number of jets for different mass points of vector-like leptons. Here vector-like lepton masses of 300, 400 and 500 GeV are considered.

the mass of the vector-like tau is higher, then its daughters carry more momentum. This implies the final state objects like leptons and jets peak at higher values. This is reflected in the distributions of H_T^{lep}, H_T^{jets} and hence, m_{eff}. Since we do not expect any large E_T^{miss} signatures in the final state, we do not see an appreciable shift in its distribution for different τ' masses. It is important to note that although figure 5.3 is the 8 TeV analog of figure 6.2, we cannot compare them. This is particularly true for H_T^{jets} and m_{eff} as the selection requirement on jet η and the overlap removal criteria are different in both the cases.

Different signal regions are considered based on different kinematic variables like H_T^{lep}, E_T^{miss}, H_T^{jets} and m_{eff}. The kinematic distributions of these variables for signal and the backgrounds is presented for $=2e/\mu+ \geq 1\tau_{had}$, on Z channel in figure 6.3. In this figure, we

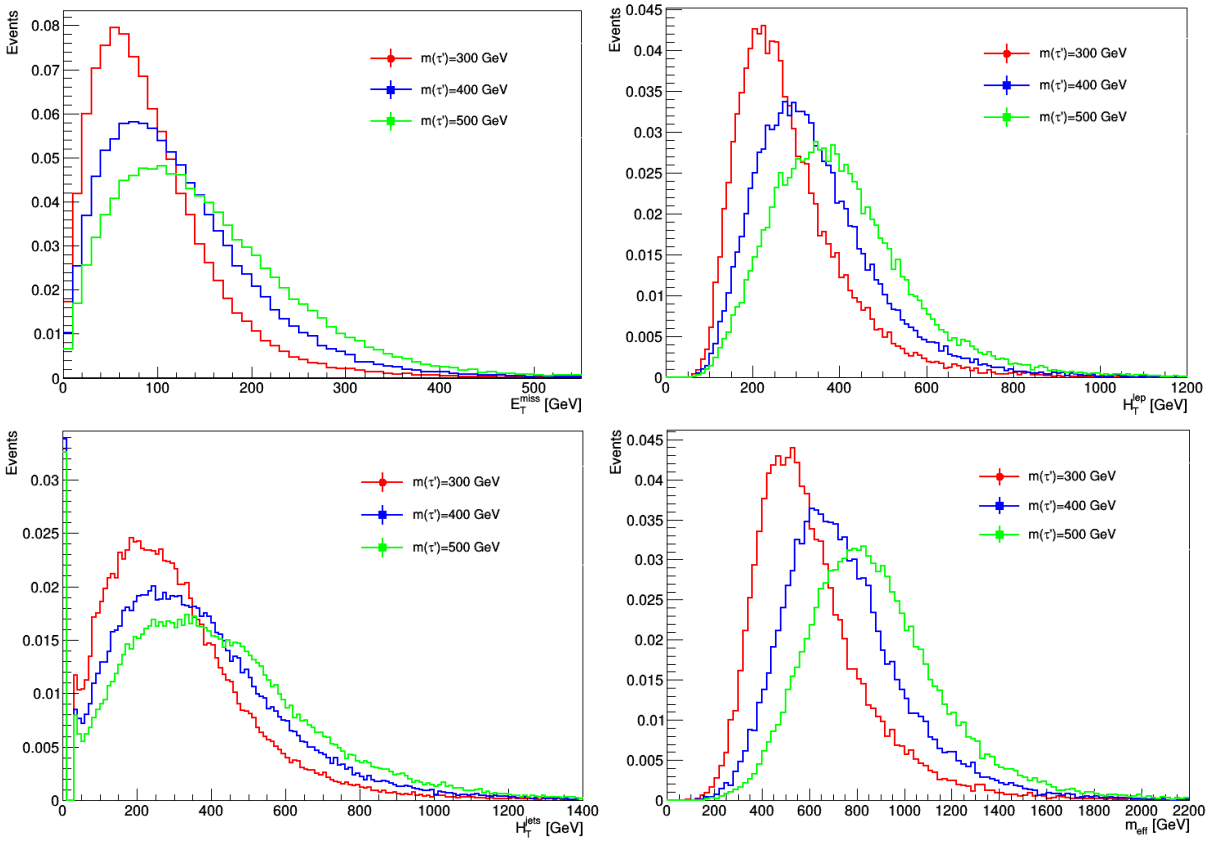

Figure 6.2: The top left panel depicts the distribution of E_T^{miss} for m(τ')=300, 400 and 500 GeV. The top right plot shows a similar comparison plot for H_T^{lep}, the bottom left panel depicts the distribution for H_T^{jets} and the bottom right plot shows the distribution of m_{eff}.

see that placing a lower threshold on these kinematic variables decreases the background considerably compared to the reduction in signal. For example, $H_T^{lep} > 500$ GeV cuts down large background as the background peaks at a lower value of H_T^{lep} than the signal. Following the same recipe, I choose different signal regions. The signal regions that I considered for the Run II analysis are listed in the Table 6.2.

6.4 Optimization of the search

The selection cuts are optimized to give maximum signal to background ratio. Here, we optimize $S/\sqrt{B}$ rather than S/B ratio because the former presents a measure of the ratio of signal events from the standard deviation in the background events. Therefore, by optimizing $S/\sqrt{B}$, we are ensuring that the chances of background fluctuations go down.

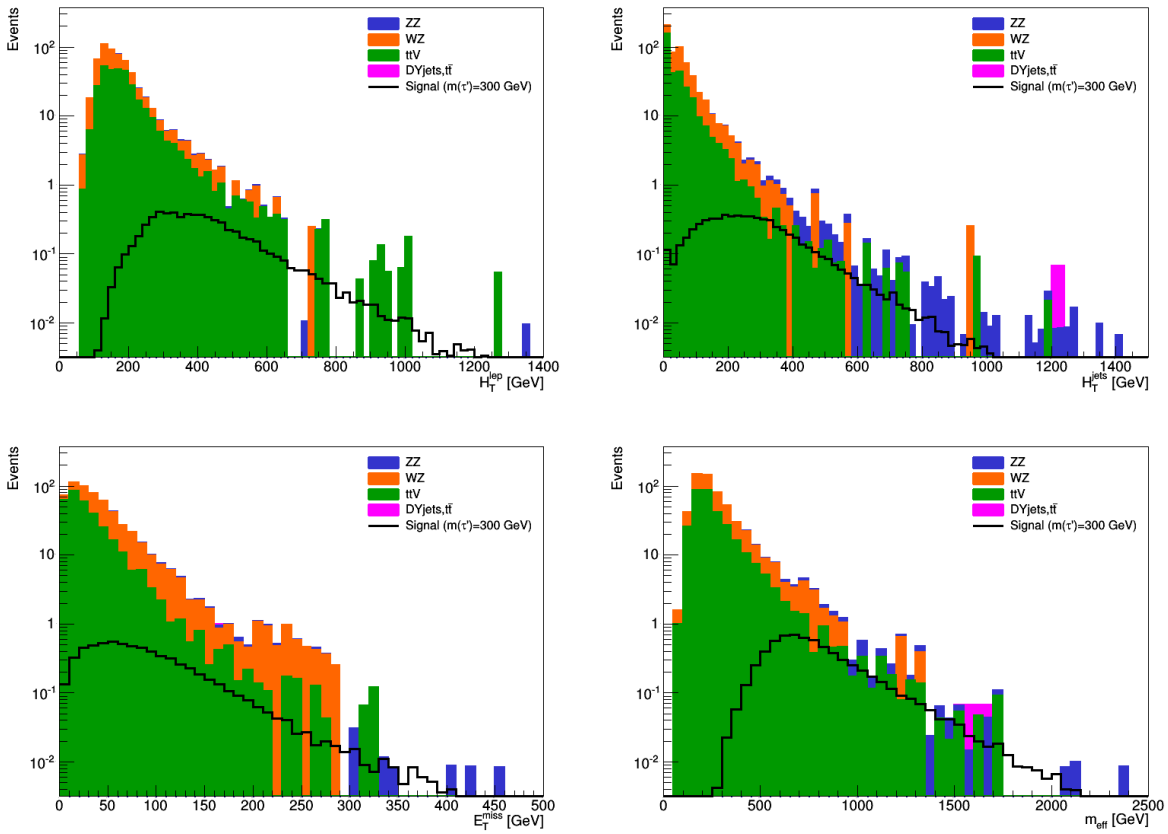

Figure 6.3: Plot showing the distributions of different kinematic variables H_T^{lep}, E_T^{miss}, H_T^{jets} and m_{eff} for the vector-like lepton signal sample ($M_{\tau'}$ = 300 GeV) and different Standard Model backgrounds. This is for the $=2e/\mu+ \geq 1\tau_{had}$, on Z channel. The signal is overlayed upon a stacked background plot for a luminosity of 20 fb^{-1}.

The plots showing comparison of $S/\sqrt{B}$ for a luminosity of 20 fb^{-1} for different signal regions in $=2e/\mu+\geq 1\tau_{had}$ channel for vector-like lepton with a mass of 300, 400 and 500 GeV are given in figure 6.4. Here, the $S/\sqrt{B}$ values are presented for different signal regions which constitute the X-ordinate in the plot. The signal region number in this plot corresponds to the signal region number in Table 6.2. From these plots, we see that the onZ channel has more senstivity to the vector-like lepton signal than the offZ channel. This is expected because during the generation of signal samples, we forced one Z boson to decay into leptons. Therefore, the signal events will predominantly dominate the onZ channel rather than the offZ channel. Therefore, the offZ channel is not sensitive though the backgrounds here are smaller. We observe that when we place a minimum cut on E_T^{miss}, $S/\sqrt{B}$ decreases. This is expected as the signal does not have any appreciable

Signal region number	Kinematic Variable Cut
0	all inclusive
1	$H_T^{leptons}$ >200 GeV
2	$H_T^{leptons}$ >500 GeV
3	E_T^{miss} ≥50 GeV
4	E_T^{miss} ≥100 GeV
5	E_T^{miss} ≥150 GeV
6	H_T^{jets} ≥100 GeV
7	H_T^{jets} ≥100 GeV, E_T^{miss} ≥50 GeV
8	H_T^{jets} ≥100 GeV, E_T^{miss} ≥100 GeV
9	H_T^{jets} ≥100 GeV, E_T^{miss} ≥150 GeV
10	m_{eff} ≥600 GeV
11	m_{eff} ≥600 GeV, E_T^{miss} ≥50 GeV
12	m_{eff} ≥600 GeV, E_T^{miss} ≥100 GeV
13	m_{eff} ≥600 GeV, E_T^{miss} ≥150 GeV
14	m_{eff} ≥400 GeV
15	m_{eff} ≥400 GeV, E_T^{miss} ≥50 GeV
16	m_{eff} ≥400 GeV, E_T^{miss} ≥100 GeV
17	m_{eff} ≥400 GeV, E_T^{miss} ≥150 GeV
18	m_{eff} ≥200 GeV
19	m_{eff} ≥200 GeV, E_T^{miss} ≥50 GeV
20	m_{eff} ≥200 GeV, E_T^{miss} ≥100 GeV
21	m_{eff} ≥200 GeV, E_T^{miss} ≥150 GeV
22	leading τ_{had} p_T ≥ 100 GeV
23	leading τ_{had} p_T ≥ 200 GeV

Table 6.2: Signal regions used for Run II analysis based on different kinematic variables such as E_T^{misS}, H_T^{lep}, H_T^{jets} and m_{eff}. The signal region number 0 refers to all inclusive channel with no cuts on these kinematic variables. The last two singal region are used only for $=2e/\mu+ \geq 1\tau_{had}$ channel.

missing energy. Upon comparing these plots, we observe that the signal region numbers 2, 10 and 23 provide high $S/\sqrt{B}$ where the selections are H_T^{lep} >500 GeV, m_{eff} >600 GeV and leading τp_T >200 GeV.

We have similar plots for $\geq 3e/\mu$ channel for m(τ')= 300, 400 and 500 GeV in figure 6.5. Note that the signal region numbers 23 and 24 are not applicable for this channel. From the plots, we notice that the signal region numbers 11 and 15. We observe that the m_{eff} >400 GeV cut in combination with E_T^{miss} >50 GeV (signal region no. 15) gives

the maximum $S/\sqrt{B}$ for m(τ')= 300 GeV. But as m(τ') increases, the signal region with m_{eff} >600 GeV in combination with E_T^{miss} >50 GeV starts to dominate. As can be observed from this figure, the most sensitive region is given by m_{eff} >600 GeV in combination with E_T^{miss} >50 GeV (signal region no. 11). This is also true for m(τ')= 500 GeV. This behavior can be explained based on figure 6.2. We noticed that as mass of the vector-like lepton increases, the peak in the m_{eff} shifts to the higher values. This implies that the signal regions including events with higher m_{eff} will be more sensitive than the ones which include lower values. Therefore, the trend seen in $S/\sqrt{B}$ values in m_{eff} signal regions is expected.

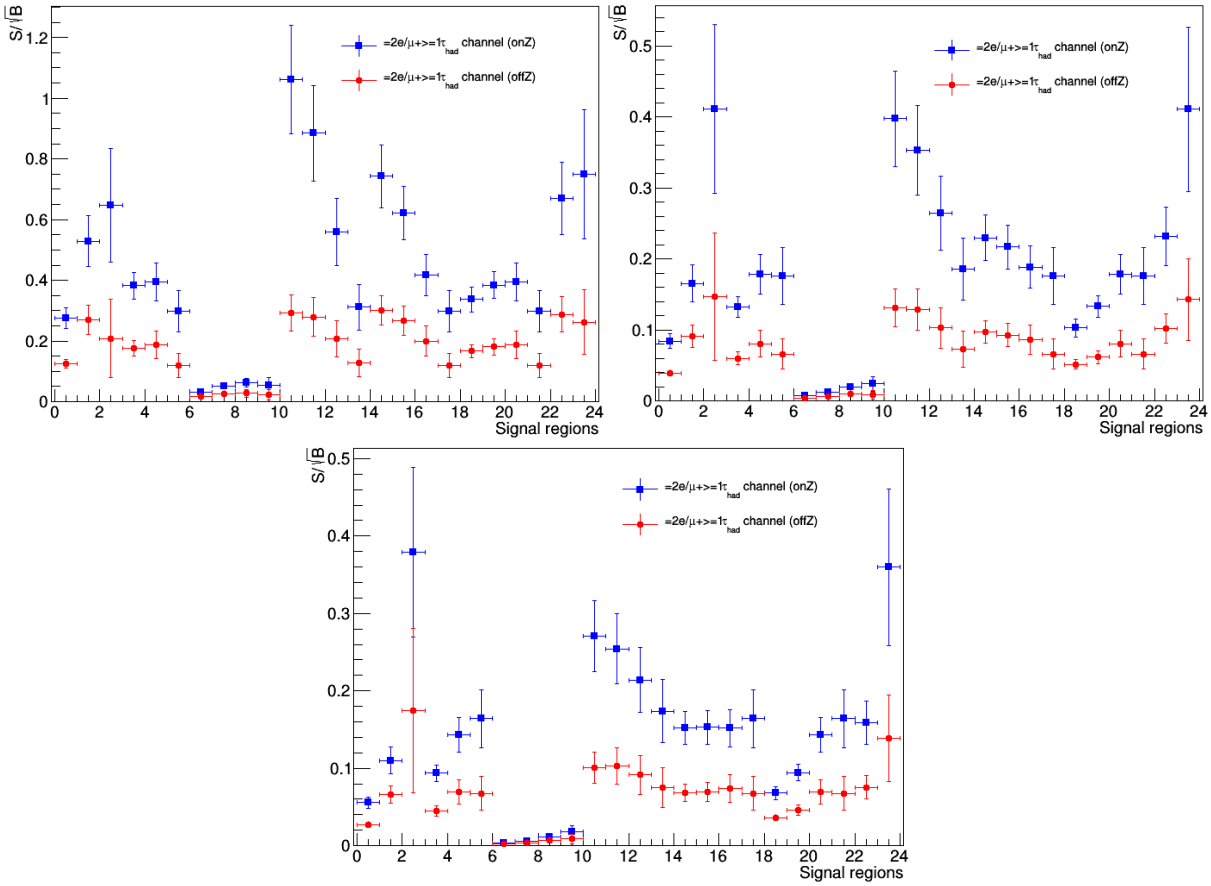

Figure 6.4: $S/\sqrt{B}$ for different signal regions of $=2e/\mu+\geq 1\tau_{had}$ channel as a function of the signal region number. The X ordinate here corresponds to the signal region number in Table 6.2. Here, m(τ') = 300 GeV for the top left plot, m(τ') = 400 GeV for the top right plot and m(τ') = 500 GeV for the bottom plot. The predictions are for luminosity of 20 fb^{-1}.

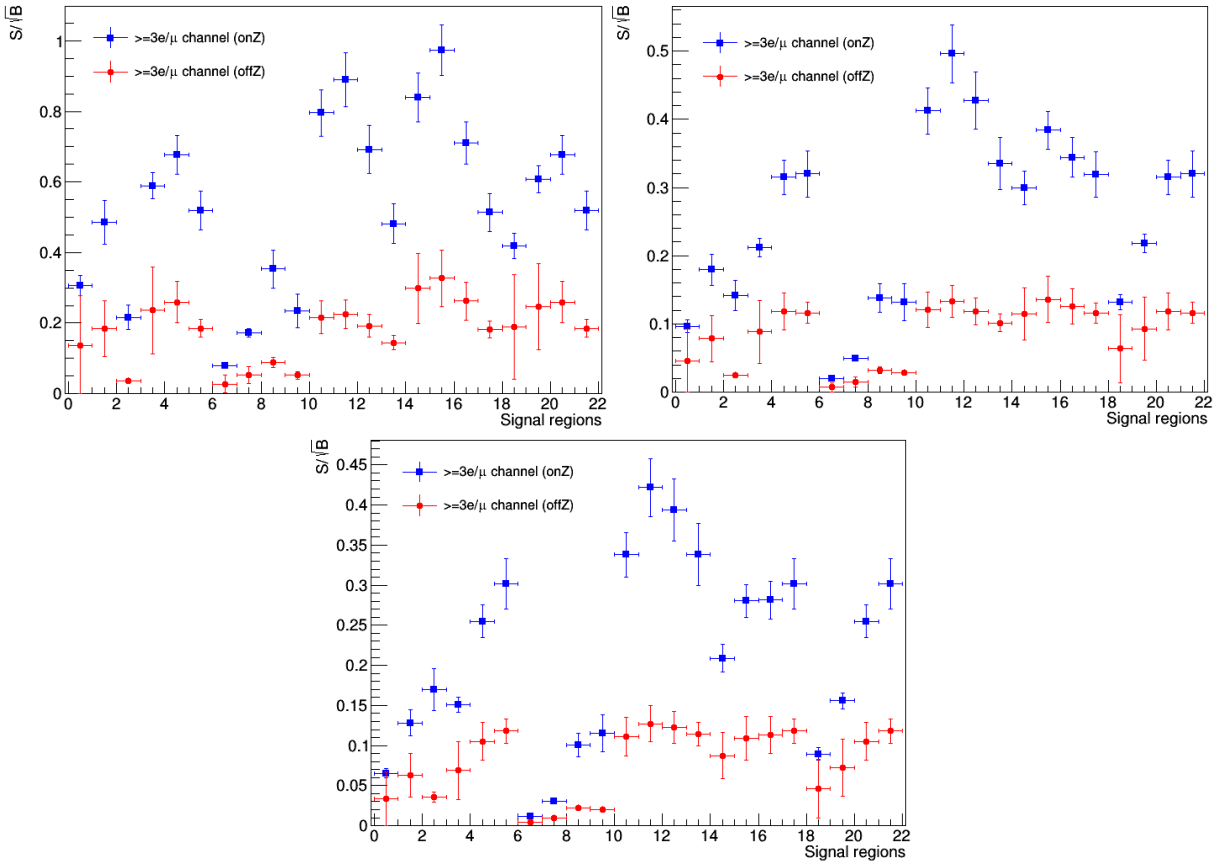

Figure 6.5: $S/\sqrt{B}$ for different signal regions of $\geq 3e/\mu$ channel as a function of the signal region number. The X ordinate here corresponds to the signal region number in Table 6.2. Here, m(τ') = 300 GeV for the top left plot, m(τ') = 400 GeV for the top right plot and m(τ') = 500 GeV for the bottom plot. The predictions are for luminosity of 20 fb^{-1}.

6.5 Prediction of exclusion limits

I calculate 95% CL exclusion limit [59, 60] using a statistical tool, RooStats [73]. The expected number of signal events, N_{exp} and the 95% exclusion limit, N_{lim} for a luminosity of 20 fb^{-1} are listed for the optimized signal regions in table 6.3. The optimized search region for $\geq 3e/\mu$, onZ channel is the one with $m_{eff} \geq 600$ GeV in combination with $E_T^{miss} \geq 50$ GeV (signal region number 11). But it does not constrain the doublet VLL model. On the other hand, the best exclusion limit is given by $m_{eff} \geq 600$ GeV (signal region number 10) for the $=2e/\mu+\geq 1\tau_{had}$, on Z channel. Using this signal region, vector like leptons with masses below 365 GeV are excluded..

The exclusion limit plot corresponding to $=2e/\mu+\geq 1\tau_{had}$, on Z channel and signal

m(τ') [GeV]	$\geq$3 e/μ, on Z channel Signal region no. 15		$= 2e/\mu+1\tau_{had}$, on Z channel Signal region no. 10	
	N_{exp}	N_{lim}	N_{exp}	N_{lim}
280	4.97	2.93	5.24	2.88
300	4.67	2.94	5.19	2.88
350	2.77	2.94	3.32	2.88
400	1.62	2.93	1.95	2.87
425	1.59	2.93	1.89	2.88
450	1.33	2.92	1.55	2.88
475	1.19	2.93	1.38	2.87
500	1.15	2.93	1.33	2.88

Table 6.3: The expected number of signal events, N_{exp} and the 95% CL upper limit on the number of events, N_{lim} for two different optimized signal regions.

Sample	$\geq$3 e/μ, on Z channel Signal region no. 15	$= 2e/\mu+1\tau_{had}$, on Z channel Signal region no. 10
	Signal	
m(τ')=280 GeV	4.97±0.12	5.24±0.12
m(τ')=300 GeV	4.67±0.10	5.19±0.11
m(τ')=350 GeV	2.77±0.06	3.32±0.06
m(τ')=400 GeV	1.62±0.03	1.95±0.04
m(τ')=425 GeV	1.59±0.03	1.89±0.04
m(τ')=450 GeV	1.33±0.03	1.55±0.03
m(τ')=475 GeV	1.19±0.02	1.38±0.02
m(τ')=500 GeV	1.15±0.02	1.33±0.02
	Background	
WZ	30.89±3.09	12.18±1.22
ZZ	22.58±8.58	8.92±3.4
ttV	2.68±0.39	2.71±0.43
$t\bar{t}$	0.094±0.094	0.076±0.076
$Z + jets$	0.094±0.094	0.076±0.076
Total background	56.34±12.25	23.96±5.19

Table 6.4: The expected number of events for different signals and backgrounds in two different signal regions for an integrated luminosity of 20 fb^{-1}.

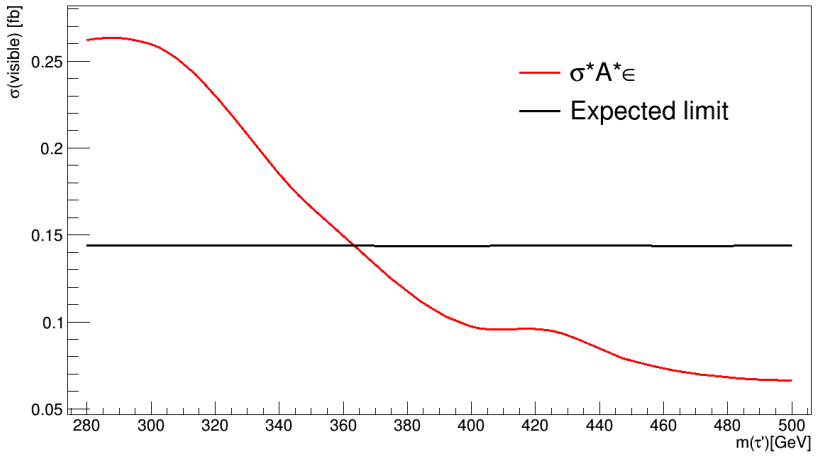

Figure 6.6: The exclusion contour showing the visible cross section corresponding to the signal and the predicted visible cross section. This plot corresponds to $2e/\mu+\geq 1\tau_{had}$, onZ channel and a signal region where m_{eff} >600 GeV. I predict that the vector-like leptons with masses below 365 GeV can be excluded with 20 fb^{-1} of Run II data.

region with m_{eff} >600 GeV is shown in figure 6.6. I conclude that vector-like leptons in the doublet model with masses below 365 GeV can be excluded at 95% CL using 20 fb^{-1} of Run II data.

Chapter 7

Summary

In this thesis, I explored the feasibility of discovering vector-like leptons in the Run I and Run II of the Large Hadron Collider.

For the Run I analysis, I interpret an ATLAS 8 TeV multilepton search result in the context of vector-like lepton models. I exclude vector-like electrons with m(e')<150 GeV within the singlet A model. This exclusion limit is comparable to the one placed in Ref. [43]. For the doublet VLL model, the lower bound on the mass of vector-like leptons is 280 GeV. There are no constraints on the singlet B model using this result. Luminosity of at least few 100 fb^{-1} is necessary to constrain this model [41].

I study the prospects of doublet VLL model in Run II of the Large Hadron Collider. The optimal search region for $\geq 3e/\mu$ and onZ channel corresponds to the one with m_{eff} $\geq$600 GeV in combination with E_T^{miss} $\geq$50 GeV. The $=2e/\mu+\geq 1\tau_{had}$, onZ channel is optimized for the signal region corresponding to m_{eff} $\geq$600 GeV. Using the latter signal region, I exclude vector-like leptons of the doublet VLL model with masses below 365 GeV for a luminosity of 20 fb^{-1}.

Bibliography

[1] Abdus Salam, J. C. Ward, Phys. Lett. 13, 168-171 (1964)

[2] S. L. Glashow, Nucl. Phys. 22 (1961) 579-588

[3] Steven Weinberg, Phys. Rev. Lett. 19 (1967) 1264-1266

[4] Particle Data Group collaboration, Chin. Phys. C38 (2014) 090001

[5] Mary K. Gaillard, Paul D. Grannis and Frank J. Sciulli, Rev. Mod. Phys. 71 (1999) S96

[6] Wikipedia: Standard Model

[7] Peter W. Higgs, Phys. Rev. Lett. 13 (1964) 508-509

[8] F. Englert, R. Brout, Phys. Rev. Lett. 13 (1964) 321-323

[9] Summary of CMS cross section measurements, http://cern.ch//go/pNj7

[10] Paul Langlacker, arXiv:0901.0241 [hep-ph]

[11] Joseph D. Lykken, CERN Yellow Report CERN-2010-002, pp. 101-109, arXiv:1005.1676 [hep-ph]

[12] The Super-Kamiokande Collaboration, Phys. Rev. Lett. Vol 81 1562-1567 (1998), arXiv:hep-ex/9807003

[13] The SNO collaboration, Phys. Rev. Lett. Vol 89, No. 1, 011302 (2002)

[14] M. N. Rebelo, arXiv:1603.01210 [hep-ph]

[15] van Albada, T. S., Bachall, J. N., Begeman, K., Sancisi, R. 1985, ApJ, 295, 305

[16] Katherine Garrett, Gintaras Duda, Adv.Astron.2011:968283,2011, arXiv:1006.2483 [hep-ph]

[17] The ATLAS collaboration, Phys. Lett. B716 (2012) 1-29, arXiv:1207.7214

[18] The CMS collaboration, Phys. Lett. B 716 (2012) 30, arXiv:1207.7235

[19] Stephen P. Martin, arXiv:hep-ph/9709356

[20] S. F. King, Rept. Prog. Phys. 67 (2004) 107-158, arXiv:hep-ph/0310204

[21] Abdel Pérez-Lorenzana, J. Phys. Conf. Ser. 18 (2005) 224-269, arXiv:hep-ph/0503177

[22] Adam Falkowski, David M. Straub, Avelino Vicente, JHEP 05 (2014) 092, arXiv:1312.5329 [hep-ph]

[23] B. Keren-Zur, P. Lodone, M. Nardecchia, D. Pappadopulo, R.Rattazzi, *et al.*, Nucl. Phys. B 867 (2013) 429-447

[24] M.Redi, JHEP 1309 (2013) 060, arXiv:1306.1525

[25] R. Contino, T. Krmaer, M. Son and R. Sundrum, JHEP 0705 (2007) 074

[26] K. Agashe, T. Okui and R. Sundrum, Phys. Rev. Lett. 102 (2009) 10801, arXiv:0810.1277

[27] Aniket Jogliker, Pedro Schwaller, Carlos E. M. Wagner, JHEP 07 (2013) 046, arXiv:1303.2969

[28] ATLAS Collaboration, ATLAS-CONF-2015-081

[29] CMS Collaboration, CMS PAS EXO-15-004

[30] Abdelhak Djouadi, John Ellis, Rohini Godbole, Jérémie Quevillon, arXiv:1601.03696 [hep-ph]

[31] ATLAS collaboration, Phys. Rev. Lett. 109 (2012) 032001, arXiv:1202.6540 [hep-ex]

[32] CMS collaboration, Phys. Lett. B 716 (2012) 103, arXiv:1203.5410 [hep-ex]

[33] CMS collaboration, JHEP 05 (2012) 123, arXiv:1204.1088 [hep-ex]

[34] CMS collaboration, Phys. Rev. D 86 (2012) 112003, arXiv:1209.1062 [hep-ex]

[35] Otto Eberhardt, Geoffrey Herbert, Heiko Lacker, *et al.*, Phys. Rev. Lett. 109 (2012) 241802, arXiv:1209.1101 [hep-ph]

[36] https://twiki.cern.ch/twiki/bin/view/CMSPublic/Hig14009TWiki

[37] L3 Collaboration, P. Achard *et al.*, Phys. Lett. B 517 (2001) 75, arXiv:hep-ex/0107015 [hep-ex]

[38] Koji Ishiwata, Mark B. Wise, Phys. Rev. D 88, 055009 (2013), arXiv:1307.1112 [hep-ph]

[39] F. del Aguila, Li. Ametller, G. L. Kane and J. Vidal, Nucl. Phys. B 334 (1990) 1-23

[40] Luca Panizzi talk at the European Centre for Theretical studies in nuclear physics and related areas http://www.ectstar.eu/sites/www.ectstar.eu/files/talks/Panizzi.pdf

[41] Nilanjana Kumar and Stephen P. Martin, Phys. Rev. D 92, 115018 (2015), arXiv:1510.03456 [hep-ph]

[42] Stephen P. Martin and James D. Wells, Phys. Rev. D 86 (2012) 035017, arXiv:1206.2956 [hep-ph]

[43] The ATLAS collaboration, JHEP 09 (2015) 108, arXiv:1506.01291 [hep-ex]

[44] The ATLAS collaboration, JHEP 08 (2015) 138, arXiv:1411.2921

[45] Johan Alwall *et al.*, JHEP 1106 (2011) 128 , arXiv:1106.0522 [hep-ph]

[46] S. Catani, Y. L. Dokshitzer, M. H. Seymour and B. R. Webber, Nucl. Phys. B 406 (1993) 187

[47] S. D. Ellis and D. E. Soper, Phys. Rev. D 48 (1993) 3160, hep-ph/9305266

[48] Y. L. Dokshitzer, G. D. Leder, S. Moretti and B. R. Webber, JHEP 9708, 001 (1997), arXiv:hep-ph/9707323

[49] M. Wobisch and T. Wengler, arXiv:hep-ph/9907280

[50] G. C. Blazey *et al.*, arXiv:hep-ex/0005012

[51] Matteo Cacciari, Gavin P. Salam, Gregory Soyez, JHEP 0804 (2008) 063, arXiv:0802.1189 [hep-ph]

[52] Gavin P. Salam, Eur. Phys. J. C67 (2010) 637-686, arXiv:0906.1833 [hep-ph]

[53] Torbjörn Sjöstrand *et al.*, Comput. Phys. Commun. 191 (2015) 159-177, arXiv:1410.3012 [hep-ph]

[54] S. Agostinelli *et al.*, Nucl. Instrum. Methods Phys. Res. 506, 250 (2003)

[55] Matteo Cacciari, Gavin P. Salam, Gregory Soyez, arXiv:1111.6097 [hep-ph]

[56] DELPHES 3 Collaboration (de Favereau, J. *et al.*), JHEP 1402 (2014) 057, arXiv:1307.6346 [hep-ex]

[57] Adam Alloul, Neil D. Christensen, Celine Degrande, Claude Duhr, Benjamin Fuks, Comput. Phys. Commun. 185 (2014) 2250-2300, arXiv:1310.1921 [hep-ph]

[58] Private communication with Joshua Ruderman. These samples were prepared in older version of MadGraph (v4.5.2)

[59] Thomas Junk, Nucl. Instrum. Meth. A434:435-443,1999, arXiv:[hep-ex]9902006

[60] A. L. Read, J. of Phys. G 28 (2002) 2693

[61] ATLAS collaboration, Phys. Rev. D 87, 052002

[62] CMS Collaboration, JHEP 08 (2011) 155, arXiv:1106.4503

[63] The ATLAS collaboration, Phys. Rev. D 87 (2013) 012008, arXiv:1208.0949

[64] CMS collaboration, Phys. Lett. B 733 (2014) 328, arXiv:1311.4937 [hep-ex]

[65] The ATLAS collaboration, Phys. Rev. D. 90, 052001 (2014), arXiv:1405.5086 [hep-ex]

[66] CMS collaboration, Phys. Rev. D 90, 032006 (2014), arXiv:1404.5801 [hep-ex]

[67] https://twiki.cern.ch/twiki/pub/CMSPublic/PhysicsResultsMUO/PlotsForApproval_52XRunAB

[68] https://twiki.cern.ch/twiki/pub/CMSPublic/PhysicsResultsMUO/SingleMuonEfficiencies_2012.p

[69] https://twiki.cern.ch/twiki/pub/CMSPublic/PhysicsResultsMUO/DP2015_047.pdf

[70] ATLAS collaboration, Eur.Phys.J. C74 (2014) 3130, arXiv:1407.3935 [hep-ex]

[71] ATLAS collaboration, arXiv:1603.05598 [hep-ex]

[72] CMS collaboration, CMS-PAS-EXO-16-002, http://cds.cern.ch/record/2140978

[73] https://twiki.cern.ch/twiki/bin/view/RooStats/WebHome